Supporting Information for

Fusion of Pyrene and Phenanthrene through 5*H*-Imidazo[1,2-*a*]azepine Scaffolds: Structural Tuning for Fluorescence Labeling and Bacterial Imaging

Nicholas P. Qiu, Ramin Eradeh, Liam H. Britt, and Yuming Zhao*

Department of Chemistry, Memorial University of Newfoundland,
Core Science Facility, 45 Arctic Avenue, St. John's, NL, Canada A1C 5S7
Tel: +1 709 864 8747, E-mail: yuming@mun.ca

Contents

1 Experimental Methods

1.1 General

Chemicals were purchased from commercial suppliers and used directly without purification. All reactions were conducted in standard, dry glassware under inert atmosphere (N_2). Pyrene-4,5-diones **1a** and **1b** were synthesized through the literature method.[1] Evaporation and concentration were carried out with a rotary evaporator. Flash column chromatography was performed with 240–400 mesh silica gel, and thin-layer chromatography (TLC) was carried out with silica gel F254 covered on plastic sheets and visualized by UV light.

1.2 NMR Characterization

^{1}H (16 scans, 10,000 Hz spectral width) and ^{13}C (broadband decoupling, 10,240 scans, 30,120 Hz spectral width) NMR spectra were measured on a Bruker Avance 500 MHz multinuclear spectrometer with DMSO-d_6 as the solvent. Chemical shifts (δ) are reported in ppm downfield relative to the signals of the internal reference $SiMe_4$ or residual solvents (Me_2SO: δ_H = 2.50 ppm, δ_C = 40.00 ppm). Coupling constants (J) are given in Hz.

1.3 MS Characterization

High resolution MALDI-TOF MS analysis was performed on a Bruker ultrafleXtreme MALDI TOF/TOF system. Spectra were collected using a laser repetition rate of 1,000 Hz with 200 shots per spectrum. The ion source voltages were set to 20 kV (source 1) and 17.7 kV (source 2), with a lens voltage of 8.4 kV. Reflector voltages were 20.8 kV and 11 kV, and the detector voltage was 2.134 kV. The instrument was operated in positive ion mode using an external calibration standard.

1.4 X-Ray Crystallography

Single-crystal X-ray diffraction (SCXRD) data was collected at 100(2) K on a XtaLAB Synergy-S, Dualflex, HyPix-6000HE diffractometer using Cu Kα radiation (λ = 1.5406 Å). Crystal was mounted on nylon CryoLoops with Paraton-N. The data collection and reduction were processed within CrysAlisPro (Rigaku OD, 2021). A multi-scan absorption correction was applied to the collected reflections. Using the Olex2 software package,[2] the structure was solved with the ShelXT[3] structure solution program using intrinsic phasing and refined with the ShelXL[4] refinement package using Least Squares minimization. All non-hydrogen atoms were refined anisotropically. The organic hydrogen atoms were generated geometrically. visualization of crystal structures was carried out using Olex2 software package.

1.5 UV-Vis and Fluorescence Spectroscopy

UV–Vis absorption spectra were recorded using an Agilent 8453 spectrophotometer equipped with the Agilent UV–Visible Chemstation Software Package. Fluorescence spectra were obtained using a Photon Technology International (PTI) Quantamaster spectrofluorometer fitted with a PTI

820 photomultiplier detection system and the PTI FELIX Fluorescence Analysis Software. All measurements were conducted in a quartz cuvette.

1.6 Quantum Yields and Fluorescence Lifetime Measurements

The determination of relative fluorescence quantum yields (ϕ) in *N*,*N*-dimethylformamide (DMF) was carried out following established protocols,[5,6] employing quinine sulfate (ϕ = 0.546) as the standard.[6] Quantum yield values were calculated according to the following equation:

$$\Phi(x) \;=\; \frac{A_s}{A_x}\,\frac{F_x}{F_s}\left(\frac{n_x}{n_s}\right)^2 \Phi(s)$$

where the subscripts x and s refer to the *sample* and the *standard*, respectively. The individual terms are defined as follows:

$\Phi(x)$: Fluorescence quantum yield of the sample.

$\Phi(s)$: Fluorescence quantum yield of the standard (known reference).

A_x: Absorbance of the sample at the excitation wavelength.

A_s: Absorbance of the standard at the same excitation wavelength.

F_x: Integrated fluorescence emission intensity of the sample.

F_s: Integrated fluorescence emission intensity of the standard.

n_x: Refractive index of the solvent in which the sample is dissolved.

n_s: Refractive index of the solvent in which the standard is dissolved.

Fluorescence lifetime measurements were carried out in DMF using the same HORIBA Scientific Fluorolog-QM instrument, operated in Multi One-to-Four Exponentials mode. Excitation was performed with 360 nm and 450 nm pulsed lasers, respectively. The acquisition parameters included a 100 ns time window, 4,096 time channels, and a peak channel count of 5,000. Time-resolved emission data were fitted to multi-exponential decay models (2–4 components), and optimal lifetimes were selected based on the goodness-of-fit criterion ($\chi^2 \approx 1$), emission reproducibility, and physical plausibility of the decay components. Among the tested excitation and emission combinations, the most consistent and reliable results were obtained using 450 nm excitation and monitoring emission at longer wavelengths (510–540 nm), where signal intensity and fitting quality were maximized. Data fitting and lifetime extraction were performed using the FelixFL software package. All measurements were conducted in a quartz cuvette.

1.7 Excitation-Emission Matrix Analyses

EEM spectra were acquired in DMF using a HORIBA Scientific Fluorolog-QM spectrofluorometer equipped with the FelixFL software package. Measurements were performed with slit widths set to 3.5 nm, a step size of 1 nm, and an integration time of 1 second. Excitation wavelengths were scanned from 290 nm to 475 nm in intervals of 10 nm, while emission wavelengths were measured from 350 nm to 750 nm. Contour plots were generated using Python and smoothed using two-dimensional linear interpolation of the raw EEM data onto a regular grid using the scipy.interpolate.griddata (method="linear") function. All measurements were conducted in a quartz cuvette.

1.8 Computational Analysis

(TD)DFT calculations[7] were conducted using the Gaussian 16 software package.[8] The applied DFT and TD-DFT methods include the hybrid functional, M06-2X,[9,10] in conjunction with the Karlsruhe basis set, def2-SVP, for all optimization, frequency and single point excited state calculations.[11,12] Solvent effects were analyzed using the Polarizable Continuum Model (PCM).[13–16] In addition, visualization of molecular structures was carried out using the PyMOL[17] and ChimeraX[18] software packages. Contour plots for frontier molecular orbitals (FMOs) were generated using VMD.[19]

1.9 BSA Titration Experiments

BSA (10μM) was dissolved in 0.1 M phosphate buffer solution. BSA titrations were carried out by adding the stock solutions of **2a** (3.00×10^{-4} M), **2b** (5.61×10^{-4} M), **3a** (9.60×10^{-4} M), and **3b** (4.47×10^{-4} M) in DMSO respectively in the prepared BSA solution (3.00 mL) using a microsyringe. UV-Vis absorption spectra were recorded on an Agilent 8453 spectrophotometer. Fluorescence spectra were measured on a Photon Technology International (PTI) Quantamaster spectrofluorometer equipped with a PTI 820 Photomultiplier Detection System and the PTI FELIX Fluorescence Analysis Software. All measurements were conducted in a quartz cuvette.

Fluorescence quenching data was analyzed by plotting the ratio F_0/F, where F_0 and F are the fluorescence intensities in the absence and presence of quencher, respectively, as a function of quencher concentration $[Q]$. The titration curves were fit to the Stern-Volmer model:[20,21]

$$\frac{F_0}{F} = 1 + K_{\mathrm{SV}}[Q]$$

For fluorescence enhancement analysis, the intensity ratio F/F_0 was plotted against titrant concentration $[S]$. The data were fit to the classical binding isotherm:[20,22]

$$\frac{F}{F_0} = 1 + \frac{a[S]}{b + [S]}$$

Where, $a = \Delta F_{\mathrm{max}}$ represents the maximum change in fluorescence, and $b = K_d$ is the dissociation constant. The binding affinity was reported as the association constant $K_a = 1/K_d$. Fitting was conducted using the nonlinear regression method implemented in the sklearn package of Python.

1.10 Bacterial Imaging Studies

For bacterial imaging, two strains were cultured: the Gram-positive *Exiguobacterium* sp. N4-1P[23] and the Gram-negative *Alcanivorax* venustensis. *Exiguobacterium* sp. N4-1P was cultured by adding 0.5 mL of bacterial suspension into 50 mL of marine broth (35.6 g/L) in 125 mL conical flasks, followed by incubation at 28 °C for 48 hours. *Alcanivorax venustensis* was cultured under the same conditions, except the marine broth was supplemented with 1.0% sodium pyruvate. A total of 21 samples were prepared for imaging: a marine broth blank, 16 bacteria combined with fluorophore samples – consisting of 100 μL of **2a** (6.0×10^{-5} M), **2b** (6.0×10^{-5} M), **3a** (1.5×10^{-5} M), and **3b** (6.0×10^{-5} M) solutions dissolved in DMF each added to 1000 μL of the respective bacterial suspensions (1:10 v/v) in 1.5 mL centrifuge tubes for each respective incubation time (four samples per fluorophore) – and 4 control samples that consisted of 100 μL DMF added to 1000 μL of the respective bacterial suspensions (1:10 v/v) in 1.5 mL centrifuge tubes for each respective incubation time. Samples were incubated for either 1 hour or 24 hours, then centrifuged (400 rcf, 5.5 min, 4 °C), and the supernatant was removed. Each pellet was re-suspended in 100 μL of growth medium, and 10 μL of each suspension was used to prepare glass slides with cover slips. Slides were visualized and photographed using a Nikon Eclipse T*i*2 microscope equipped with a Nikon Digital Sight 50M camera under a 385 nm LED illuminator and NIS Elements Basic Research Imaging Software. Photo editing was completed using the NIS Elements Basic Research Imaging Software.

1.11 Molecular Docking and Dynamic Simulations with BSA

Molecular docking and molecular dynamics simulations were conducted using the YASARA Structure software package.[24] The simulation cell was defined as a cube (10.00 Å) surrounding the protein with periodic boundaries set. Molecular docking simulations were performed using the `dock_run.mcr` macro (298.00 K, pH = 7.4), which uses the VINA Is Not Autodock (VINA) docking engine and automatically fills the cell with water molecules. Molecular dynamics were performed using the `md_run.mcr` macro (298.00 K, pH = 7.4) which also fills the cell with water molecules. MD simulations were run for > 40 ns. Binding energies were conducted using the `md_analyzebindenergy.mcr` macro. BSA structures (PDB ID: 4F5S) were acquired from the RCSB PDB Protein Data Bank. The Chain A of BSA was extracted and optimized/cleaned using the PyMOL software package.[17] The ligand structures were optimized at the M06-2X/Def2SVP level using the Gaussian 16 software package[8] and then converted into PDB files for use in YASARA. Plots were generated using the YASARA program, while structural analysis, interaction mapping, and MD visualization were performed using BIOVIA Discovery Studio Visualizer[25] and PyMOL,[17] respectively. Molecular dynamics movies were also generated using the YASARA `md_play.mcr` macro.

1.12 Synthesis

6*H*-phenanthro[4,5-*cde*]pyreno[4',5':4,5]imidazo[1,2-*a*]azepin-6-one (2a)

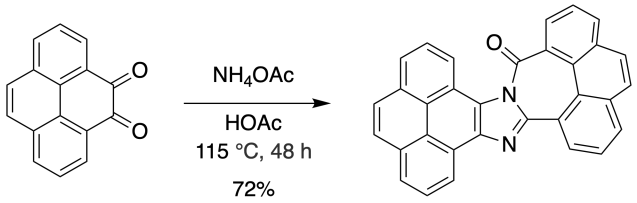

1a **2a**

Pyrene-4,5-dione (**1a**, 1.00 g, 4.31 mmol), ammonium acetate (3.99 g, 51.8 mmol), and glacial acetic acid (99.7%, 55.5 mL) were added to a 150 mL round-bottom flask. The reaction mixture was refluxed, stirred and heated at 115 °C for 48 hours. Next the reaction was cooled to room temperature yielding a brown mixture with a pale brown-yellow precipitate. Next, 60 mL of water was added to the round-bottom flask, followed by suction filtration of the mixture. The resulting brown-yellow powdery solid residue was then washed with 50 mL of methanol. The solid was then purified by column chromatography over 240-400 mesh silica gel. Column chromatography was performed using gradient elution (hexanes/diethyl ether, 100:0, then 90:10, 80:20 to flush the less polar impurities followed by hexanes/dichloromethane, 90:10, then 80:20, then 50:50, then 0:100). This yielded pure compound **2a** (0.689 g, 1.55 mmol, 72%) as a yellow solid. NMR and HR-MS have been reported previously.[26]

4,9,14,18-Tetra-*tert*-butyl-6*H*-phenanthro[4,5-*cde*]pyreno[4',5':4,5]imidazo[1,2-*a*]azepin-6-one (2b)

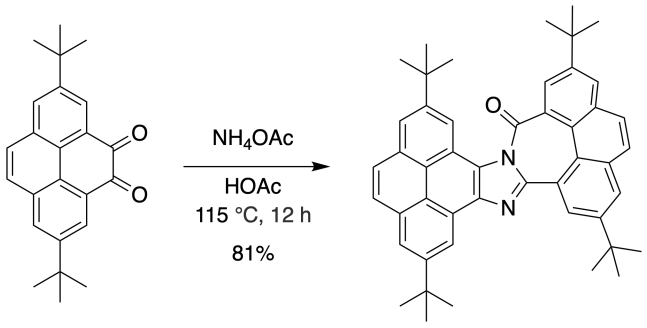

1b **2b**

2,7-Di-*tert*-butylpyrene-4,5-dione (**1b**, 1.00 g, 2.90 mmol), ammonium acetate (2.24 g, 29.0 mmol), and glacial acetic acid (99.7%, 55.5 mL) were added to a 150 mL round-bottom flask. The reaction mixture was refluxed, stirred and heated at 115 °C for 12 hours. Next the reaction mixture was taken off and cooled to room temperature resulting in a brown mixture with yellow precipitate. Next, 60 mL of water was added to the round-bottom flask, followed by suction filtration of the mixture. The resulting residue was a yellow powdery solid. The solid was then purified by column chromatography over 240-400 mesh silica gel. Column chromatography was performed using gradient elution (hexanes/diethyl ether, 100:0, then 85:15, 75:25). This yielded pure compound **2b** (0.787 g, 1.18 mmol, 81%) as a yellow crystalline solid.NMR and HR-MS have been reported previously.[26]

6*H*-phenanthro[4,5-*cde*]pyreno[4',5':4,5]imidazo[1,2-a]azepin-6-ol (3a)

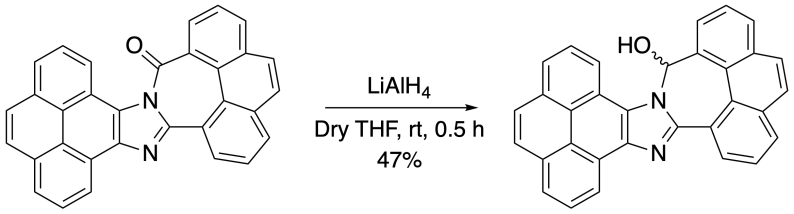

2a **3a**

2a (0.100 g, 0.225 mmol), $LiAlH_4$ (42.7 mg, 1.12 mmol), and 50 mL dry THF a 100 mL round-bottom flask under inert atmosphere (N_2). The reaction mixture was stirred at room temperature for 30 minutes. After the reaction was completed, 10 mL of ethyl acetate was added to the reaction flask to quench, followed by evaporating the solvent off using a rotary evaporator until 2 mL was remaining. Following, 10 mL methanol, 10 mL H_2O and 10 mL NaOH (1M) was added to the round bottom flask. The resulting mixture was suction filtered resulting in crude product which appeared as a pale brown powdery solid. The solid was then purified by column chromatography over 240-400 mesh silica gel. Column chromatography was performed using gradient elution (hexanes/dichloromethane, 100:0, then 75:25, then 50:50, then 0:100 followed by dichloromethane/methanol, 95:5). This yielded pure compound **3a** (0.048 g, 0.106 mmol, 47%) as an off-white powdery solid. ^{1}H NMR (500 MHz, $(CD_3)_2SO$): δ 9.31 (d, J = 7.83 Hz, 1H), 8.92 (dd, J = 7.64, 0.98 Hz, 1H), 8.84 (dd, J = 7.46, 1.38 Hz, 1H), 8.41-8.37 (m, 2H), 8.34-8.26 (m, 6H), 8.19 (dd, J = 8.04, 0.98 Hz, 1H), 8.16 (t, J = 7.62 Hz, 1H), 8.08 (d, J = 8.75 Hz, 1H), 8.02 (d, J = 8.77 Hz, 1H), 7.99 (t, J = 7.62 Hz, 1H), 7.86 (t, J = 7.43 Hz, 1H), 7.45 (d, J = 3.91 Hz, 1H); ^{13}C NMR (125 MHz, $(CD_3)_2SO$): δ 151.73, 138.61, 137.42, 134.38, 133.24, 132.45, 131.81, 130.38. 130.13, 129.99, 129.60, 128.54, 128.38, 128.27, 127.78, 127.25, 127.61, 127.18, 127.14, 127.02, 126.91, 126.87, 126.39, 126.11, 125.25, 125.07, 122.99, 122.59, 122.43, 119.82, 199.70, 82.48. HRMS (MALDI-TOF/TOF, positive mode) calculated for $C_{32}H_{18}N_2O$: m/z = 446.142; found 446.103 ([M + H]$^+$).

4,9,14,18-Tetra-*tert*-butyl-6*H*-phenanthro[4,5-*cde*]pyreno[4',5':4,5]imidazo[1,2-*a*]azepin-6-ol (3b)

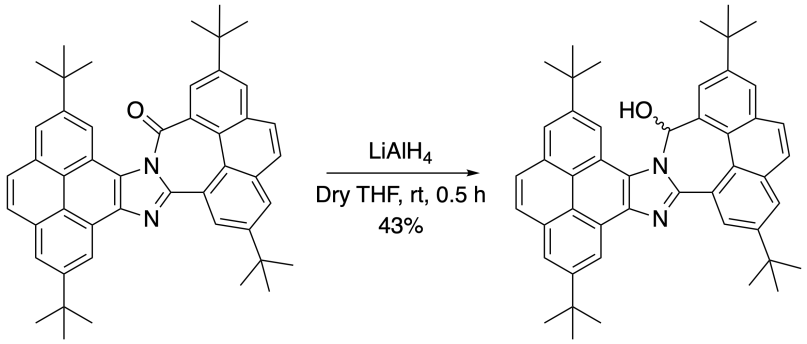

2b **3b**

2b (0.100 g, 0.149 mmol), $LiAlH_4$ (42.7 mg, 1.12 mmol), and 50 mL dry THF a 100 mL round-bottom flask under inert atmosphere (N_2). The reaction mixture was stirred at room temperature for 30 minutes. After the reaction was completed, 10 mL of ethyl acetate was added to the

reaction flask to quench, followed by evaporating the solvent off using a rotary evaporator until 2 mL was remaining. Following, 10 mL methanol, 10 mL H_2O and 10 mL NaOH (1M) was added to the round bottom flask. The resulting mixture was suction filtered resulting in crude product which appeared as a pale brown powdery solid. The solid was then purified by column chromatography over 240-400 mesh silica gel. Column chromatography was performed using gradient elution (hexanes/dichloromethane, 100:0, then 75:25, then 50:50, then 0:100 followed by dichloromethane/methanol, 95:5). This yielded pure compound **3b** (0.043 g, 0.064 mmol, 43%) as an off-white powdery solid. ^{1}H NMR (500 MHz, $(CD_3)_2SO$): δ 9.03 (d, J = 2.25 Hz, 1H), 8.95 (d, J = 1.93 Hz, 1H), 8.40 (d, J = 1.36 Hz, 1H), 8.33 (d, J = 1.92 Hz, 1H), 8.31 (s, 1H), 8.26 (d, J = 2.24 Hz, 1H), 8.23 (d, J = 4.62 Hz, 1H), 8.21 (s, 2H), 8.18 (d, J = 2.03 Hz, 1H), 8.09 (d, J = 2.02 Hz, 1H), 8.06 (d, J = 8.88 Hz, 1H), 8.00 (d, J = 8.82 Hz, 1H), 7.36 (d, J = 4.32 Hz, 1H), 1.77 (s, 9H), 1.62 (s, 9H), 1.61 (s, 9H), 1.52 (s, 9H); ^{13}C NMR (125 MHz, $(CD_3)_2SO$): δ 152.11, 149.67, 149.29, 148.94, 148.76, 138.79, 136.88, 134.61, 133.39, 132.29, 131.59, 129.37, 129.33, 129.03, 128.55, 128.40, 127.99, 127.05, 126.93, 126.33, 126.16, 125.89, 124.82, 124.80, 124.36, 122.35, 122.10, 121.20, 120.60, 116.55, 115.87, 83.48, 35.84, 35.59, 35.17, 35.02, 32.32, 32.20, 31.78, 31.58. Note that in the ^{13}C NMR, one aromatic peak is absent likely due to coincidental overlap. HRMS (MALDI-TOF/TOF, positive mode) calculated for $C_{48}H_{50}N_2O$: m/z = 670.392; found 670.399 ($[M + H]^+$).

2 NMR Spectra for New Compounds

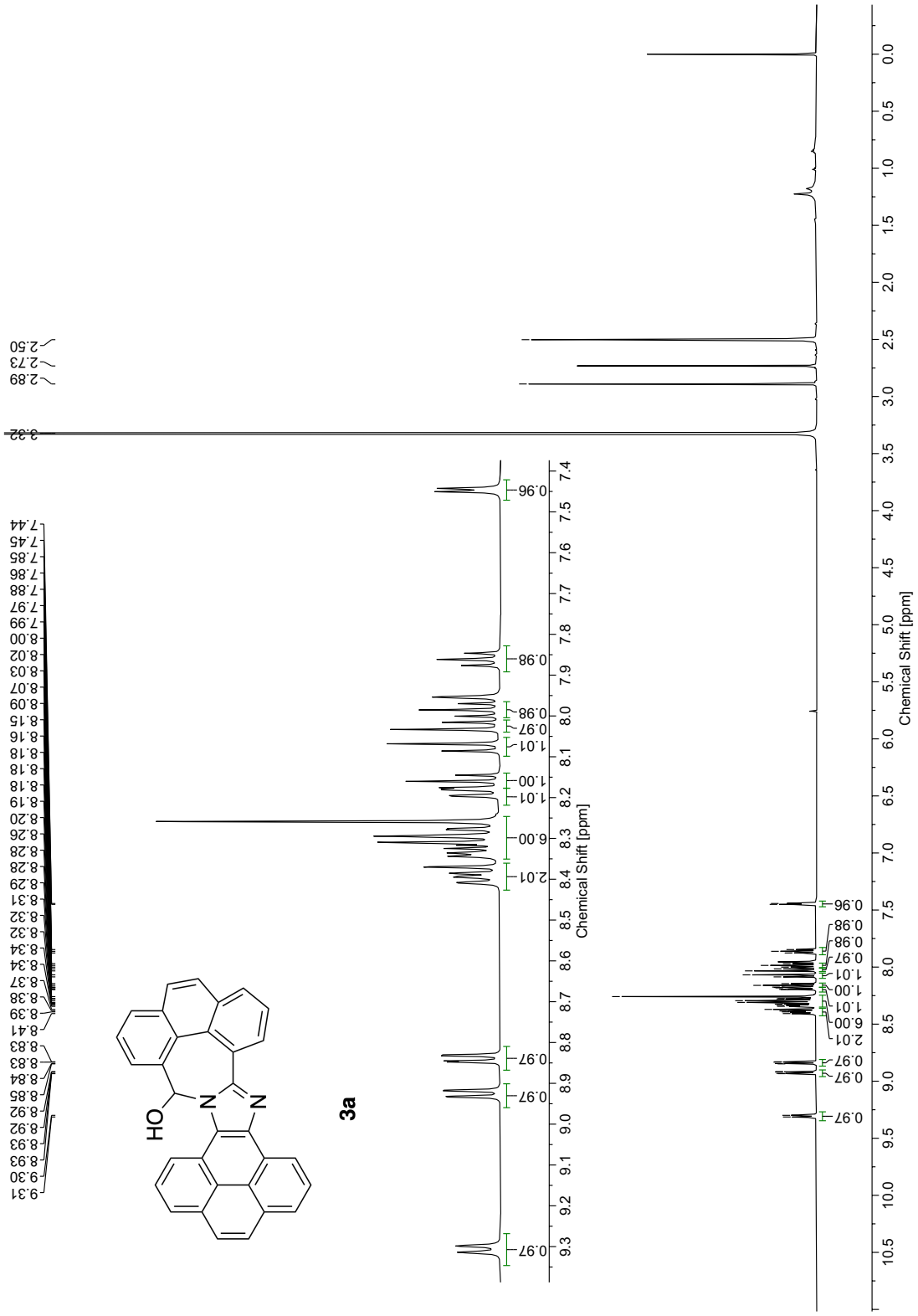

Figure S-1: ^{1}H NMR (500 MHz, DMSO-d_6) of compound **3a**.

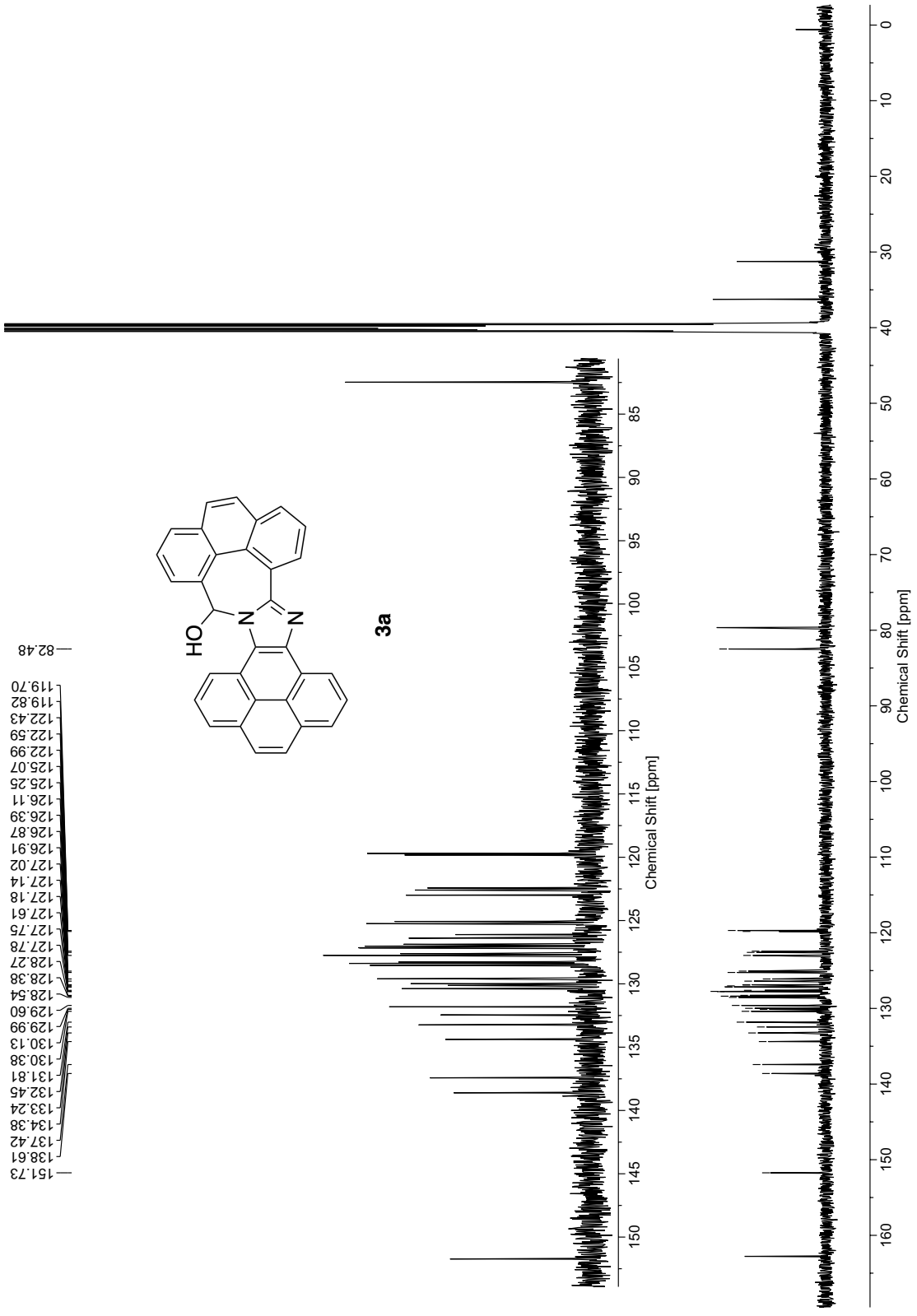

Figure S-2: $^{13}C\{^{1}H\}$ NMR (125 MHz, DMSO-d_6) of compound **3a**.

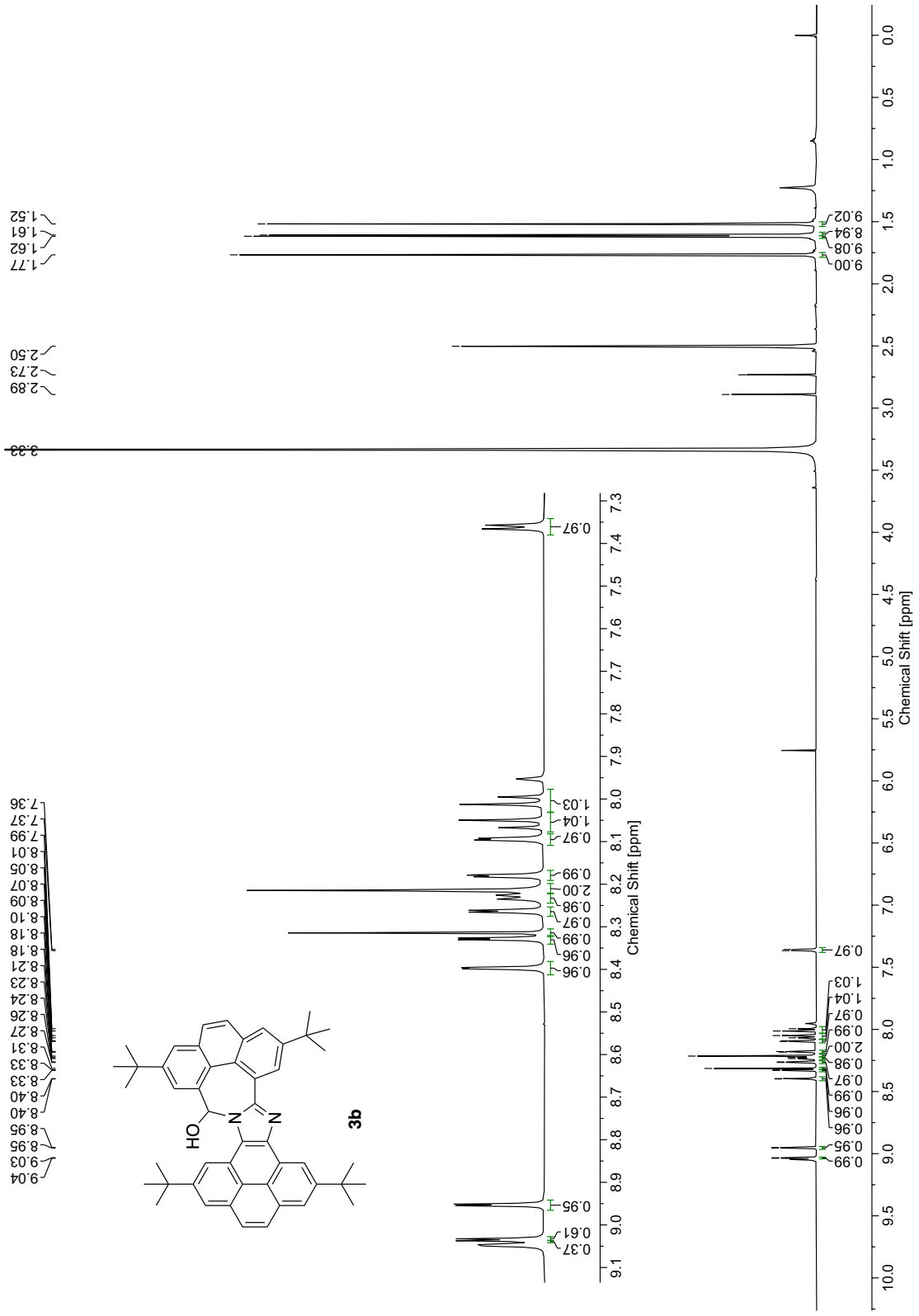

Figure S-3: ^{1}H NMR (500 MHz, DMSO-d_6) of compound **3b**.

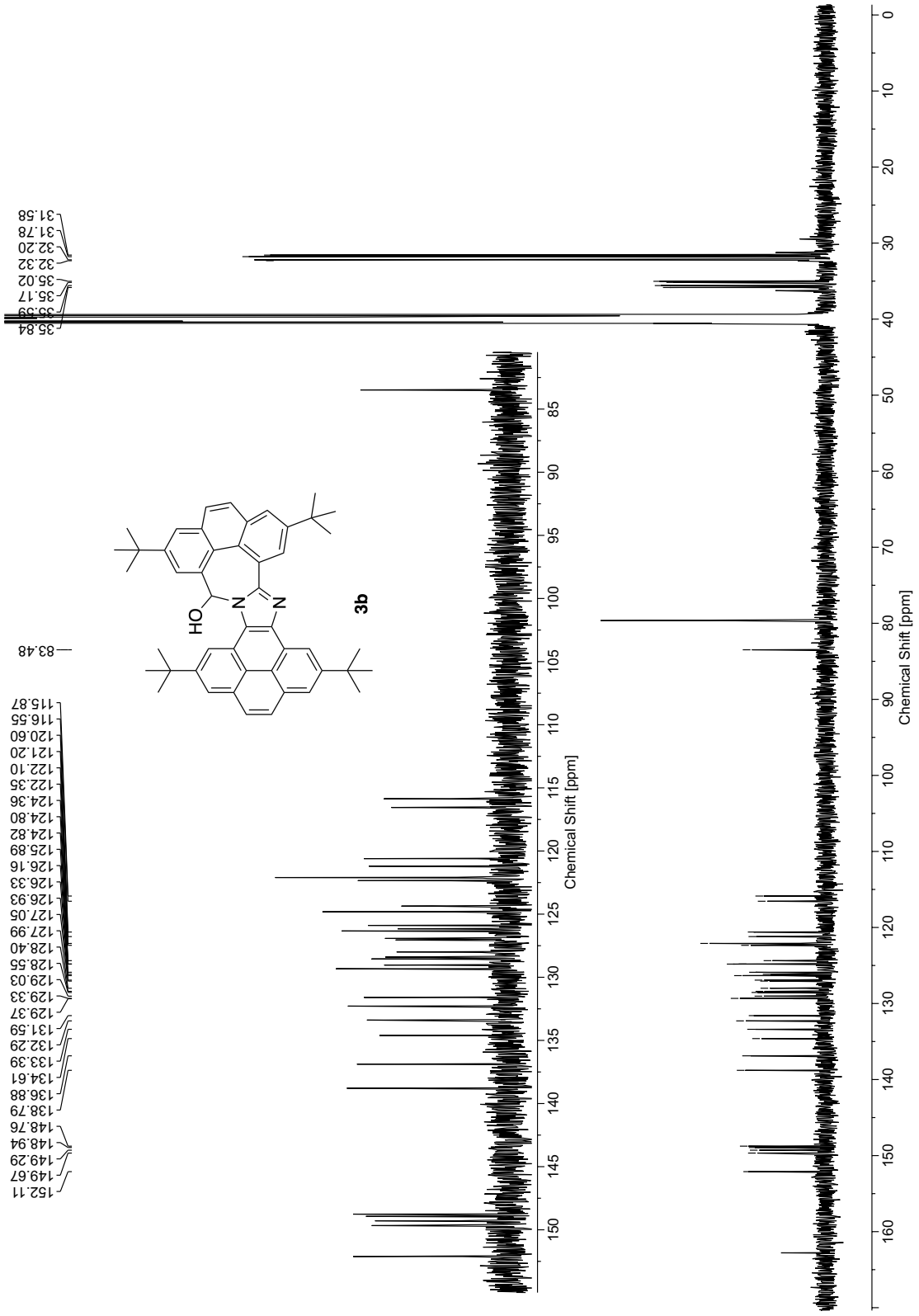

Figure S-4: $^{13}C\{^{1}H\}$ NMR (125 MHz, DMSO-d_6) of compound **3b**.

3 Single-Crystal X-Ray Diffraction Data and Structure Refinement Information

Table S-1: Crystal data and structure refinement information for **2a**

CCDC Number	2256234
Empirical formula	$C_{32}H_{16}N_2O$
Formula weight	444.47
Temperature (K)	100(2)
Crystal system	Monoclinic
Space group	Pn
a (Å)	3.95070(10)
b (Å)	17.9552(4)
c (Å)	13.8102(4)
β (°)	96.658(2)
Volume (Å^3)	973.03(4)
Z	2
ρ_{calc} (g/cm^3)	1.517
μ (mm^{-1})	0.727
F(000)	460.0
Crystal size (mm^3)	0.287 × 0.044 × 0.032
Radiation	Cu Kα ($\lambda = 1.54184$ Å)
2θ range (°)	4.922 to 158.776
Index ranges	$-4 \leq h \leq 4$, $-22 \leq k \leq 22$, $-17 \leq l \leq 17$
Reflections collected	19374
Independent reflections	3747 [$R_{\text{int}} = 0.0506$, $R_\sigma = 0.0386$]
Data/restraints/parameters	3747 / 44 / 429
Goodness-of-fit on F^2	1.036
Final R indexes [I $\geq 2\sigma$(I)]	$R_1 = 0.0517$, $wR_2 = 0.1337$
Final R indexes [all data]	$R_1 = 0.0619$, $wR_2 = 0.1424$
Largest diff. peak/hole (e Å^{-3})	0.29 / −0.21

Table S-2: Crystal data and structure refinement information for **2a + BARF**

CCDC Number	2430322
Empirical formula	$C_{50}H_{18}BF_{15}N_2O_2$
Formula weight	974.47
Temperature (K)	100(2)
Crystal system	Monoclinic
Space group	$P2_1/c$
a (Å)	15.61620(10)
b (Å)	7.91840(10)
c (Å)	30.8317(3)
α (°)	90
β (°)	97.4280(10)
γ (°)	90
Volume (Å^3)	3780.51(7)
Z	4
ρ_{calc} (g/cm^3)	1.712
μ (mm^{-1})	1.373
$F(000)$	1952.0
Crystal size (mm^3)	0.086 × 0.063 × 0.050
Radiation	Cu Kα ($\lambda = 1.54184$ Å)
2θ range (°)	5.708 to 159.412
Index ranges	$-18 \leq h \leq 19$, $-10 \leq k \leq 9$, $-39 \leq l \leq 37$
Reflections collected	49661
Independent reflections	8087 [$R_{int} = 0.0354$, $R_\sigma = 0.0240$]
Data/restraints/parameters	8087 / 0 / 639
Goodness-of-fit on F^2	1.026
Final R indexes [I $\geq 2\sigma$(I)]	$R_1 = 0.0403$, $wR_2 = 0.1040$
Final R indexes [all data]	$R_1 = 0.0505$, $wR_2 = 0.1110$
Largest diff. peak/hole (e Å^{-3})	0.62 / -0.24

Table S-3: Crystal data and structure refinement information for **3a**

CCDC Number	2430295
Empirical formula	$C_{32}H_{18}N_2O$
Formula weight	446.48
Temperature (K)	110(2)
Crystal system	Orthorhombic
Space group	Pbca
a (Å)	12.4359(3)
b (Å)	15.9420(6)
c (Å)	21.1245(4)
Volume (Å^3)	4188.0(2)
Z	8
ρ_{calc} (g/cm^3)	1.416
μ (mm^{-1})	0.676
F(000)	1856.0
Crystal size (mm^3)	0.128 × 0.092 × 0.019
Radiation	Cu Kα ($\lambda = 1.54184$ Å)
2θ range (°)	8.372 to 158.378
Index ranges	$-15 \leq h \leq 15$, $-20 \leq k \leq 19$, $-26 \leq l \leq 19$
Reflections collected	21301
Independent reflections	4433 [$R_{int} = 0.0828$, $R_\sigma = 0.0627$]
Data/restraints/parameters	4433 / 1 / 320
Goodness-of-fit on F^2	1.037
Final R indexes [I $\geq 2\sigma$(I)]	$R_1 = 0.0565$, $wR_2 = 0.1329$
Final R indexes [all data]	$R_1 = 0.0890$, $wR_2 = 0.1500$
Largest diff. peak/hole (e Å^{-3})	0.34 / −0.32

4 Results of Photophysical Characterizations

4.1 EEM and Fluorescence Lifetime Measurements

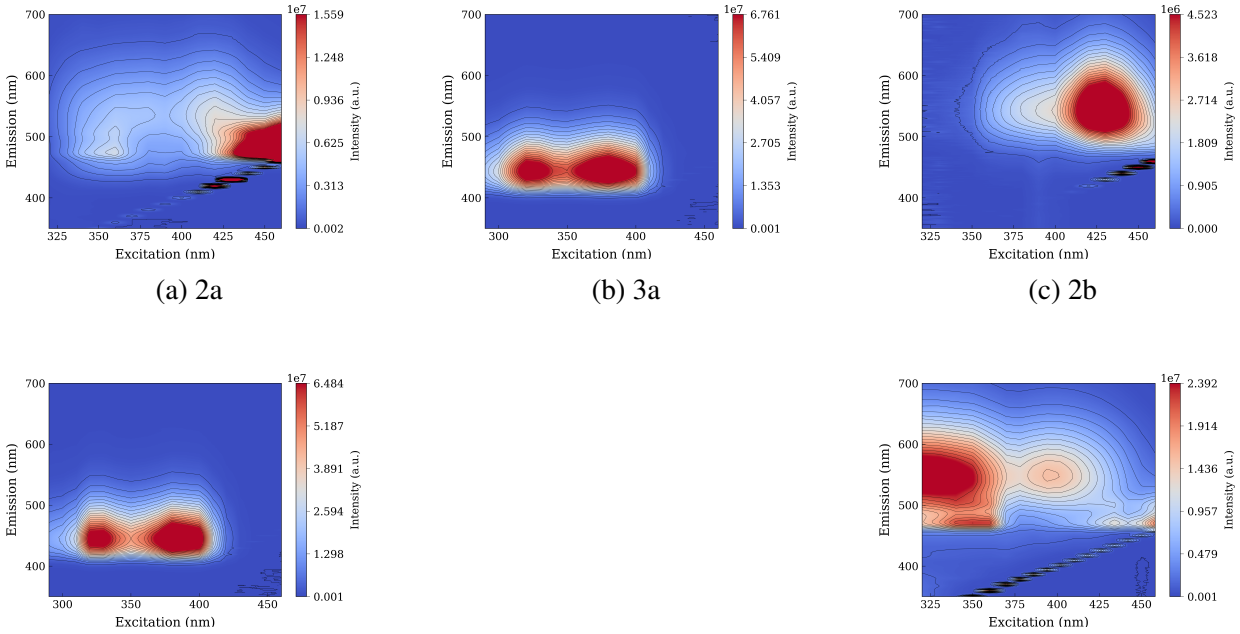

(a) 2a (b) 3a (c) 2b

(d) 3b (e) 2a + $B(C_6F_5)_3$

Figure S-5: Excitation-emission matrix (EEM) plots for **2a**, **2b**, **3a**, **3b**, and **2a**/BARF (1:1 complex) measured in DMF.

Table S-4: Fluorescence lifetimes with percentage contributions

Entry	τ_1 (ns)	Weight % τ_1	τ_2 (ns)	Weight % τ_2	χ^2
2a	0.64 ± 0.01	82.8 ± 1.0 %	4.53 ± 0.02	17.2 ± 0.12 %	1.187
2b	0.80 ± 0.01	99.1 ± 0.5 %	3.56 ± 0.21	0.9 ± 0.13 %	1.127
3a	4.05 ± 0.005	100 ± 0.14 %			1.109
3b	4.11 ± 0.005	100 ± 0.14 %			1.257
2a + BARF	0.21 ± 0.04	56.5 ± 9.7 %	1.77 ± 0.03	37.7 ± 0.4 %	1.379

Table S-5: Summary of fluorescence quantum yields (Φ_f) of **2a** + BARF (7.5×10^{-6} M), measured in DMF and DCM at room temperature

Entry	Solvent	Φ_f
2a + BARF	DMF	0.018
2a + BARF	DCM	0.023

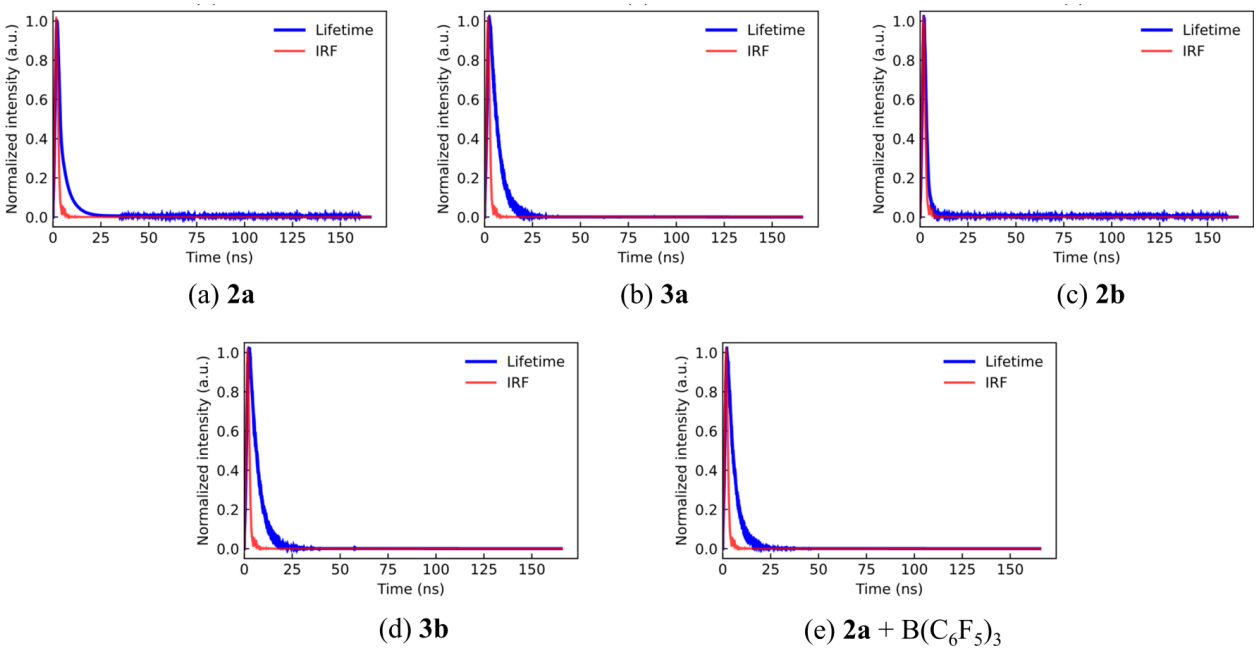

(a) **2a** (b) **3a** (c) **2b**

(d) **3b** (e) **2a** + $B(C_6F_5)_3$

Figure S-6: Fluorescence decay traces with intrument response functions (IRFs) for (a) **2a**, (b) **3a**, (c) **2b**, (d) **3b**, (e) **2a**/BARF (1:1 complex) measured in DMF.

4.2 UV-Vis Absorption and Fluorescence Spectroscopic Data

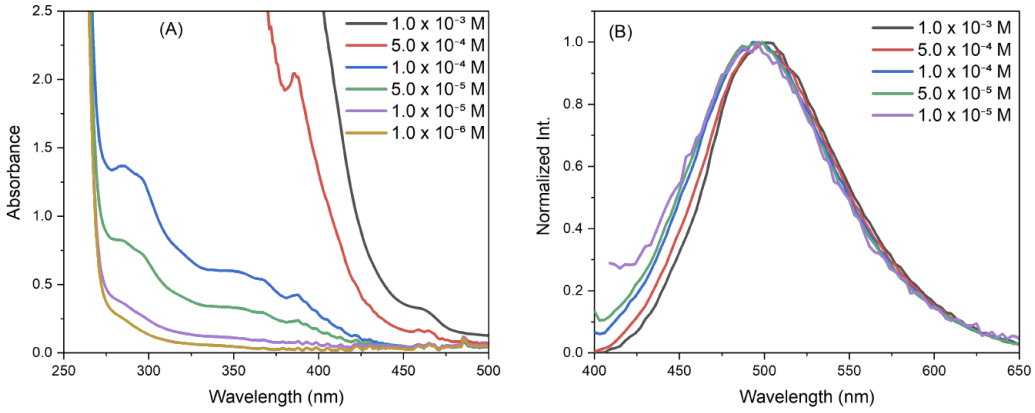

Figure S-7: (A) UV-Vis absorption spectra of **2a** measured at varied concentrations in DMF. (B) Normalized fluorescence spectra of **2a** measured at varied concentrations in DMF (λ_{ex} = 380 nm).

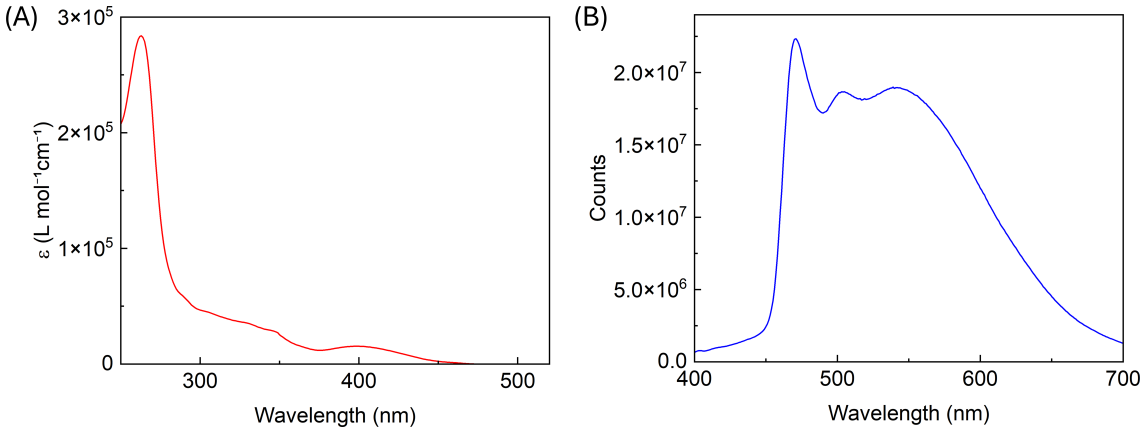

Figure S-8: (A) UV-Vis absorption spectrum of **2a** (1.0×10^{-5} M) mixed with 1 mole equivalent of BARF in DMF. (B) Fluorescence spectrum of **2a** (1.0×10^{-5} M) mixed with 1 mole equivalent of BARF in DMF (λ_{ex} = 360 nm).

Table S-6: Summary of UV–Vis absorption and fluorescence data for compound **2a**

Solvent	**UV–Vis absorption** $\lambda_{\max}$/nm	**Fluorescence** λ_{em}/nm
Acetone	389	507
ACN	**	477
Benzene	389	525
CH_2Cl_2	386	543
DMF	391	534
DMSO	391	533
EtOAc	388	513
EtOH	389	**
Hexane	386	**
MeOH	388	439
THF	**	524

** Too weak to be determined accurately

Table S-7: Summary of UV–Vis absorption and fluorescence data for compound **2b**

Solvent	**UV–Vis absorption** λ_{max}/nm	**Fluorescence** λ_{em}/nm
Acetone	390	546
ACN	388	556
Benzene	394	529
CH_2Cl_2	392	553
DMF	391	549
DMSO	392	554
EtOAc	391	532
EtOH	391	558
Hexane	393	514
MeOH	390	501
THF	392	530

** Too weak to be determined accurately

Table S-8: Summary of UV–Vis Absorption and Fluorescence Data of Compound **3a**

Solvent	**UV–Vis absorption** λ_{max}/nm	**Fluorescence** λ_{em}/nm
Acetone	387	446
ACN	387	453
Benzene	390	449
CH_2Cl_2	388	457
DMF	389	451
DMSO	388	452
EtOAc	388	443
EtOH	385	444
Hexane	**	**
MeOH	384	446
THF	388	444

** Too weak to be determined accurately

Table S-9: Summary of UV–Vis absorption and fluorescence data for compound **3b**

Solvent	**UV–Vis absorption** λ_{max}/nm	**Fluorescence** λ_{em}/nm
Acetone	389	448
ACN	388	454
Benzene	390	450
CH_2Cl_2	385	458
DMF	389	452
DMSO	390	453
EtOAc	389	445
EtOH	386	446
Hexane	391	444
MeOH	393	450
THF	390	448

** Too weak to be determined accurately

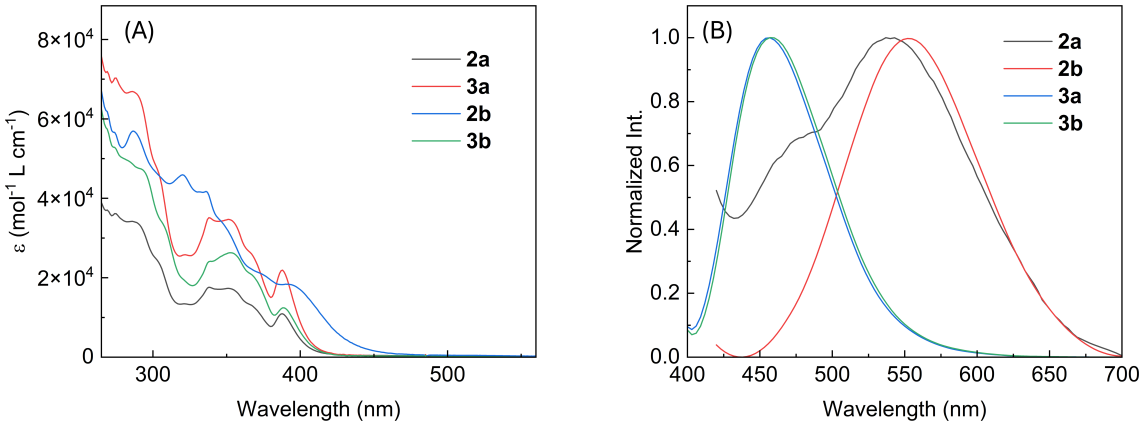

Figure S-9: (A) UV-Vis absorption spectra of **2a** (2.25×10^{-5} M), **2b** (1.11×10^{-5} M), **3a** (1.12×10^{-5} M), and **3b** (1.49×10^{-5} M) measured in CH_2Cl_2. (B) Normalized fluorescence spectra of **2a**, **2b**, **3a**, and **3b** measured in CH_2Cl_2 (λ_{ex} = 390 nm).

The fluorescence quantum yields (Φ_f) of **2a**, **2b**, **3a** and **3b** are 0.102, 0.119, 0.099, and 0.120, respectively.

Table S-10: Summary of absorption wavelengths (λ, nm) and molar extinction coefficients (ϵ, mol^{-1} L cm^{-1}) of **2a/b** and **3a/b** measured in CH_2Cl_2

Entry	λ ($\epsilon \times 10^4$)
2a	387 (1.09), 368 (1.25), 338 (1.78), 305 (2.42), 289 (3.40)
2b	395 (1.80), 373 (2.15), 351 (3.21), 337 (4.16), 320 (4.61), 287 (5.77)
3a	388 (2.17), 368 (2.53), 353 (3.46), 338 (3.49), 305 (4.66), 288 (6.69)
3b	389 (1.26), 369 (2.02), 354 (2.63), 338 (2.43), 309 (3.25), 293

Table S-11: Summary of absorption wavelengths (λ, nm) and molar extinction coefficients (ϵ, mol^{-1} L cm^{-1}) of **2a/b** and **3a/b** measured in DMF

Entry	λ ($\epsilon \times 10^4$)
2a	391 (1.67), 366 (1.91), 316 (3.42), 285 (6.54)
2b	391 (1.82), 369 (2.13), 317 (3.93), 285 (6.67)
3a	389 (1.52), 368 (1.65), 353 (2.01), 342 (2.01), 304 (3.03), 285 (5.44)
3b	389 (1.53), 369 (2.12), 354 (2.58), 343 (2.50), 309 (3.49), 286 (6.35)

5 Excitation Spectral Analysis

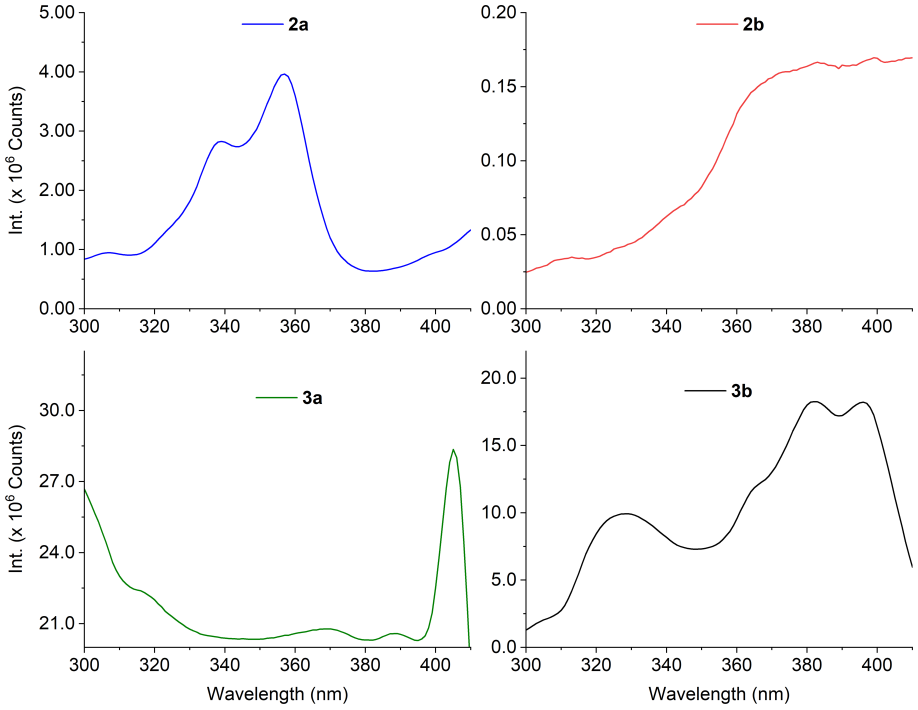

Figure S-10: Excitation spectra of **2a/b** and **3a/b** recorded in DMF solution. The spectra were acquired by monitoring the fluorescence emission intensity at 480 nm while scanning the excitation wavelength.

6 Results of DFT and TD-DFT Calculations

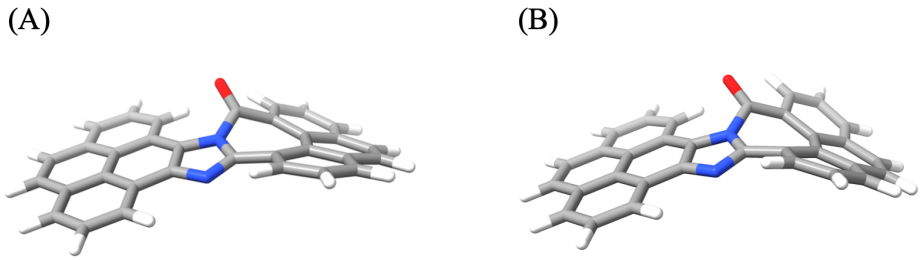

Figure S-11: (A) Optimized ground-state geometry of **2a** in the gas phase at the M06-2X/Def2-SVP level. (B) Optimized first-excited-state geometry of **2a** in the gas phase at the TD/M06-2X/Def2-SVP level.

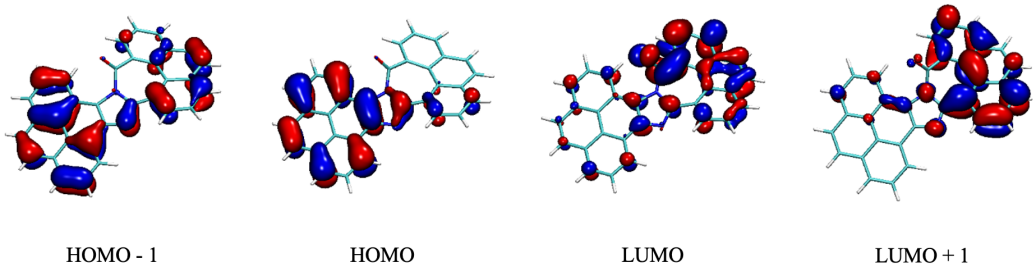

Figure S-12: Frontier molecular orbitals of **2a** (isovalue = 0.03) calculated at the M06-2X/Def2-SVP level.

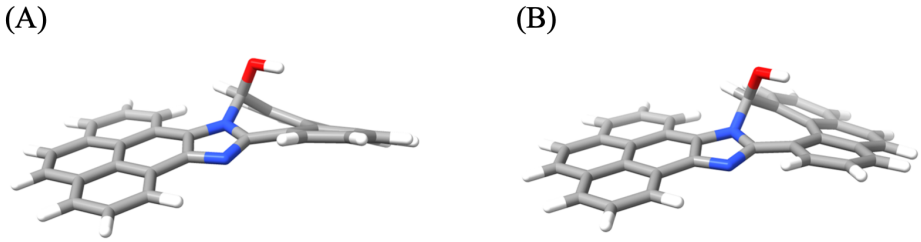

Figure S-13: (A) Optimized ground-state geometry of **3a** in the gas phase at the M06-2X/Def2-SVP level. (B) Optimized first-excited-state geometry of **3a** in the gas phase at the TD/M06-2X/Def2-SVP level.

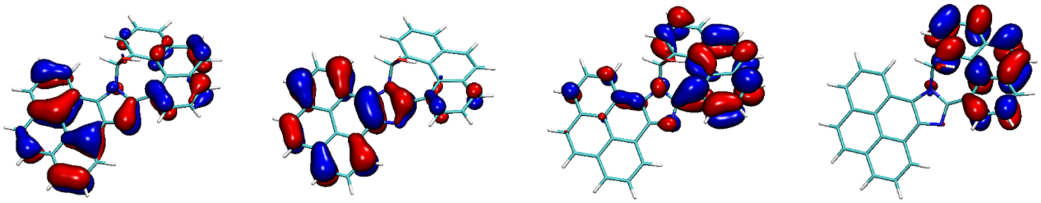

Figure S-14: Frontier molecular orbitals of **3a** (isovalue = 0.03) calculated at the M06-2X/Def2-SVP level.

Table S-12: Cartesian coordinates, energies and dipole moments of optimized geometries of **2a** in DMF

2a S_0 (E = -1412.30225402 Hartree, μ = 4.8648 Debye)				**2a** S_1 (E = -1412.28545005 Hartree, μ = 5.3718 Debye)			
C	2.81475	-3.50997	0.08663	C	2.5898	-3.50646	-0.59039
C	4.13207	-3.08348	-0.00472	C	3.93669	-3.13924	-0.5845
C	1.77026	-2.5876	0.15722	C	1.59831	-2.55898	-0.38128
C	4.43159	-1.71333	-0.06512	C	4.31839	-1.79452	-0.39855
C	3.3783	-0.75577	-0.01122	C	3.32364	-0.80344	-0.19881
C	2.02573	-1.21056	0.14012	C	1.93492	-1.1991	-0.16131
C	5.79506	-1.26201	-0.19936	C	5.7039	-1.40799	-0.42202
C	6.09562	0.05586	-0.30594	C	6.07468	-0.10723	-0.27483
C	3.70189	0.64225	-0.14409	C	3.71413	0.56787	-0.05699
C	5.05633	1.0538	-0.29675	C	5.09022	0.92273	-0.09601
C	1.02808	-0.16574	0.21196	C	0.99865	-0.17151	0.05712
C	1.32918	1.17142	0.02168	C	1.35706	1.20589	0.14837
C	2.68215	1.63391	-0.15538	C	2.74595	1.60255	0.10748
C	5.3502	2.41952	-0.44713	C	5.45838	2.28004	0.03551
C	3.00355	2.98308	-0.31566	C	3.14147	2.93225	0.22938
C	4.33638	3.37149	-0.4581	C	4.50141	3.26986	0.19578
H	4.94791	-3.80718	-0.04794	H	4.71249	-3.89149	-0.73783
H	2.58629	-4.57624	0.10531	H	2.31221	-4.54718	-0.75992
H	0.7519	-2.95976	0.22074	H	0.55241	-2.8632	-0.39628
H	6.58403	-2.01614	-0.22069	H	6.45484	-2.1868	-0.56596
H	7.13076	0.38561	-0.41271	H	7.12817	0.17695	-0.29696
H	6.39224	2.724	-0.56141	H	6.5183	2.53973	0.00592
H	4.58364	4.42695	-0.5792	H	4.80468	4.31238	0.29445
H	2.19888	3.71905	-0.3222	H	2.37607	3.69963	0.3522
N	-0.36056	-0.19386	0.33235	N	-0.38978	-0.19314	0.1473
N	0.19898	1.93772	0.03007	N	0.29097	1.98184	0.26859
C	-0.80346	1.1144	0.21458	C	-0.79856	1.16352	0.23235
C	-1.12534	-1.25526	0.88403	C	-1.06452	-1.20428	0.9069
C	-2.43834	-1.55579	0.24779	C	-2.47889	-1.48972	0.56767
C	-3.4439	-0.62031	-0.14123	C	-3.45411	-0.57458	0.02679
C	-3.37563	0.83022	0.0451	C	-3.32301	0.85478	-0.07861
C	-2.19465	1.5855	0.33561	C	-2.11625	1.63731	0.19815
C	-4.58965	1.57374	-0.08204	C	-4.47606	1.62176	-0.46573
C	-2.28922	2.94633	0.63223	C	-2.21876	3.07022	0.31919
C	-3.50669	3.62894	0.60658	C	-3.37365	3.74641	0.02227
C	-4.64042	2.95086	0.21643	C	-4.49108	3.02447	-0.4235
C	-4.6564	-1.18421	-0.64375	C	-4.71149	-1.18235	-0.34239
C	-5.81046	-0.36242	-0.88113	C	-5.78676	-0.38486	-0.84356
C	-5.79282	0.94902	-0.55925	C	-5.67975	0.96421	-0.88763
C	-2.62538	-2.92736	0.09194	C	-2.77911	-2.83584	0.76214
C	-3.78107	-3.44591	-0.49864	C	-4.00373	-3.39448	0.38098
C	-4.78619	-2.57427	-0.8528	C	-4.94707	-2.56259	-0.18346
O	-0.63936	-1.94797	1.73643	O	-0.42486	-1.85492	1.69194
H	-5.59773	3.46667	0.12575	H	-5.40567	3.5431	-0.71513
H	-1.36942	3.48159	0.85943	H	-1.3217	3.60891	0.61647
H	-3.54463	4.68957	0.85552	H	-3.41337	4.83267	0.1081
H	-6.68228	1.5699	-0.67606	H	-6.5125	1.58226	-1.22728
H	-6.71159	-0.83622	-1.27291	H	-6.70658	-0.88631	-1.14879
H	-5.72155	-2.94758	-1.27321	H	-5.91519	-2.95561	-0.49987
H	-3.89008	-4.52049	-0.64367	H	-4.19552	-4.45746	0.52304
H	-1.8417	-3.60135	0.43733	H	-2.0069	-3.46913	1.19803

Table S-13: Cartesian coordinates, energies and dipole moments of optimized geometries of **3a** in DMF

3a S_0 (E = -1413.4997428 Hartree, μ = 5.0985 Debye)				**3a** S_1 (E = -1413.48437004 Hartree, μ = 5.1345 Debye)			
C	2.83234	-3.4952	0.35834	C	-2.62279	3.55334	-0.15826
C	4.14796	-3.07213	0.24176	C	-3.96883	3.18821	-0.15024
C	1.78627	-2.57102	0.34839	C	-1.62914	2.58451	-0.09971
C	4.44218	-1.70957	0.0688	C	-4.34891	1.82908	-0.1304
C	3.38717	-0.75324	0.04573	C	-3.35341	0.82031	-0.08229
C	2.03506	-1.1971	0.2344	C	-1.96361	1.20952	-0.0196
C	5.80382	-1.26725	-0.10635	C	-5.73523	1.44798	-0.17871
C	6.0993	0.03799	-0.32506	C	-6.10533	0.13887	-0.20592
C	3.70495	0.63046	-0.20405	C	-3.74298	-0.55841	-0.12647
C	5.05776	1.03093	-0.3963	C	-5.1199	-0.90523	-0.19246
C	1.03217	-0.15484	0.23905	C	-1.02201	0.16211	0.07126
C	1.32993	1.17067	-0.05807	C	-1.38381	-1.22311	-0.03451
C	2.68127	1.6151	-0.29125	C	-2.77361	-1.60676	-0.12707
C	5.34925	2.37978	-0.66158	C	-5.48945	-2.26761	-0.25178
C	3.00143	2.94672	-0.56277	C	-3.1714	-2.93984	-0.1912
C	4.3326	3.3248	-0.74538	C	-4.53249	-3.27002	-0.25225
H	4.96632	-3.79407	0.25749	H	-4.74673	3.95282	-0.18685
H	2.60486	-4.55764	0.45195	H	-2.34485	4.60581	-0.22092
H	0.76878	-2.95044	0.39629	H	-0.58388	2.88771	-0.1569
H	6.59556	-2.0177	-0.06639	H	-6.4876	2.23836	-0.20059
H	7.13326	0.36007	-0.46272	H	-7.15969	-0.14017	-0.24759
H	6.39008	2.67538	-0.80624	H	-6.55045	-2.51984	-0.30141
H	4.57608	4.36739	-0.95468	H	-4.83599	-4.31601	-0.3006
H	2.19501	3.6784	-0.62327	H	-2.40581	-3.71684	-0.19058
N	-0.33556	-0.16328	0.44562	N	0.34533	0.16452	0.19944
N	0.20336	1.93719	-0.0589	N	-0.31636	-2.00343	-0.00618
C	-0.77946	1.1144	0.24251	C	0.76007	-1.17057	0.11265
C	-1.18069	-1.15422	1.11136	C	1.11744	1.07537	1.06497
C	-2.29689	-1.59353	0.19386	C	2.35047	1.56657	0.36267
C	-3.32877	-0.69729	-0.21497	C	3.384	0.66107	-0.06176
C	-3.33189	0.7475	0.042	C	3.30679	-0.78471	-0.03186
C	-2.1849	1.54755	0.36335	C	2.09774	-1.60715	0.14545
C	-4.57438	1.43919	-0.09117	C	4.5217	-1.52152	-0.25794
C	-2.33842	2.89797	0.67575	C	2.23293	-3.03684	0.26267
C	-3.58756	3.52408	0.65723	C	3.43947	-3.67571	0.13965
C	-4.68869	2.8041	0.24585	C	4.58416	-2.9204	-0.15602
C	-4.46525	-1.27962	-0.84758	C	4.60091	1.29371	-0.50362
C	-5.65318	-0.50279	-1.07263	C	5.75732	0.50704	-0.79316
C	-5.72552	0.7784	-0.64577	C	5.72905	-0.83815	-0.63279
C	-2.34605	-2.93702	-0.14064	C	2.48748	2.93539	0.24145
C	-3.41537	-3.46872	-0.87759	C	3.64979	3.52333	-0.29271
C	-4.4723	-2.64801	-1.20079	C	4.69572	2.69728	-0.63484
O	-1.62582	-0.68424	2.34353	O	1.38283	0.46627	2.28891
H	-0.54045	-2.00964	1.3351	H	0.45837	1.92108	1.28396
H	-2.42	-0.14536	2.22475	H	2.18088	-0.07553	2.21218
H	-5.66595	3.28137	0.15553	H	5.54565	-3.41044	-0.3169
H	-1.44153	3.46941	0.91071	H	1.32223	-3.60448	0.44265
H	-3.6759	4.57737	0.92428	H	3.50146	-4.75955	0.2428
H	-6.64467	1.35616	-0.75551	H	6.62019	-1.44085	-0.8167
H	-6.50771	-0.98835	-1.54653	H	6.6668	1.01552	-1.11812
H	-5.3495	-3.04641	-1.71355	H	5.63521	3.11395	-1.00326
H	-3.42626	-4.5259	-1.14345	H	3.72687	4.60576	-0.39264
H	-1.55088	-3.60198	0.20224	H	1.67903	3.57889	0.59625

7 Results of Fluorescence Titrations with BSA

7.1 Stern Volmer Plots

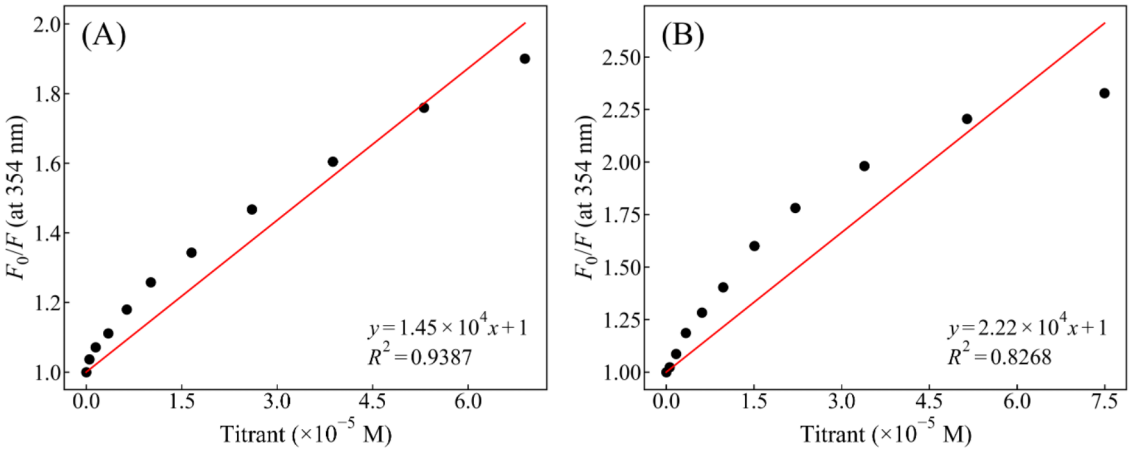

Figure S-15: Linear fitted Stern–Volmer fluorescence quenching plots of BSA with increasing concentrations of (A) **2a** (K_{SV} = 1.45 × 10^4 M^{-1}) and (B) **2b** (K_{SV} = 2.22 × 10^4 M^{-1}).

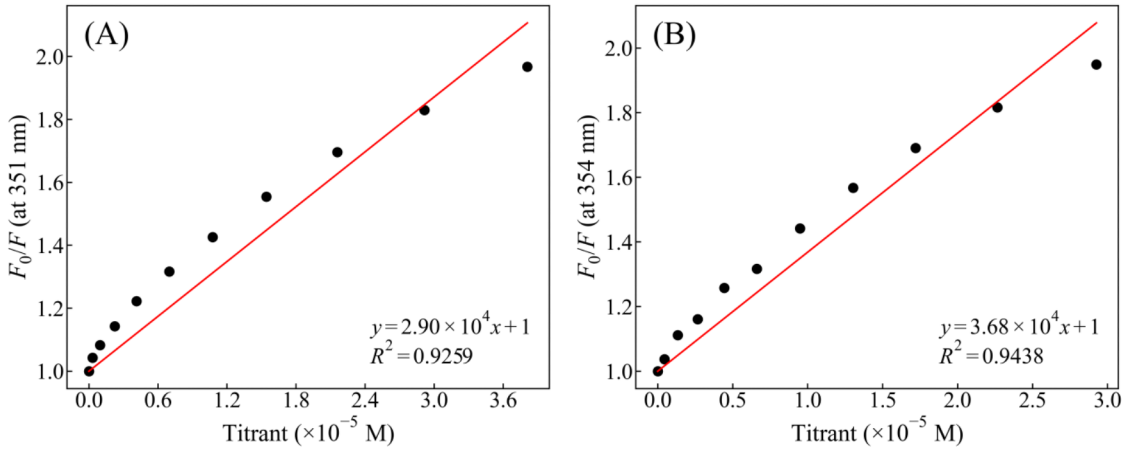

Figure S-16: Linear fitted Stern–Volmer fluorescence quenching plots of BSA with increasing concentrations of (A) **3a** (K_{SV} = 2.90 × 10^4 M^{-1}) and (B) **3b** (K_{SV} = 3.68 × 10^4 M^{-1}).

The titration curves were also fit to a nonlinear Stern–Volmer model:[20,21]

$$\frac{F_0}{F} = 1 + \frac{a[Q]}{b + [Q]}$$

The apparent Stern–Volmer constant was calculated as $K_{SV} = a/b$, which reflects the quenching efficiency.

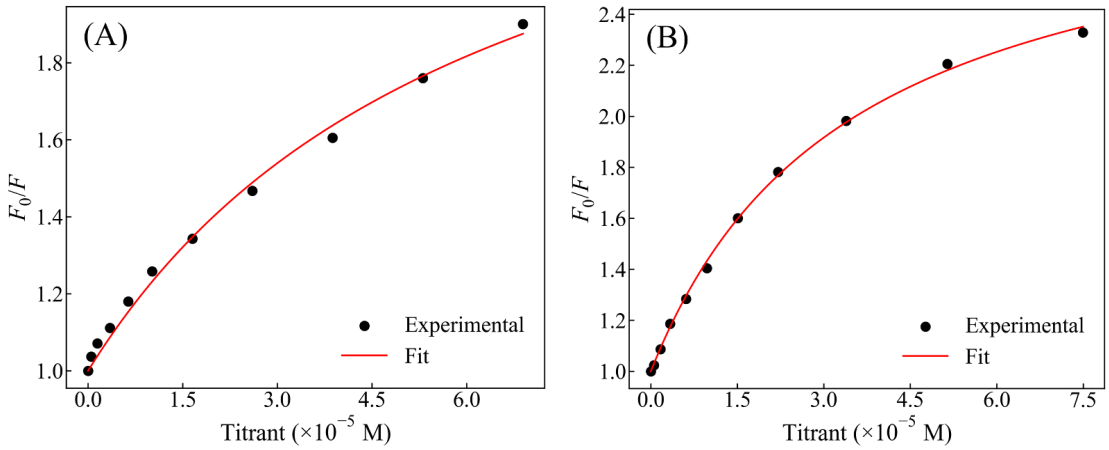

Figure S-17: Non-linear fitted Stern–Volmer fluorescence quenching plots of BSA with increasing concentrations of (A) **2a** ($a = 1.68 \pm 0.156$, $b = 6.37 \times 10^{-5} \pm 9.95 \times 10^{-6}$, R^2 = 0.9938) and (B) **2b** ($a = 1.98 \pm 0.0465$, $b = 3.47 \times 10^{-5} \pm 1.69 \times 10^{-6}$, R^2 = 0.9989). Measurements for (A) and (B) were taken at $\lambda_{ex} = 277$ nm.

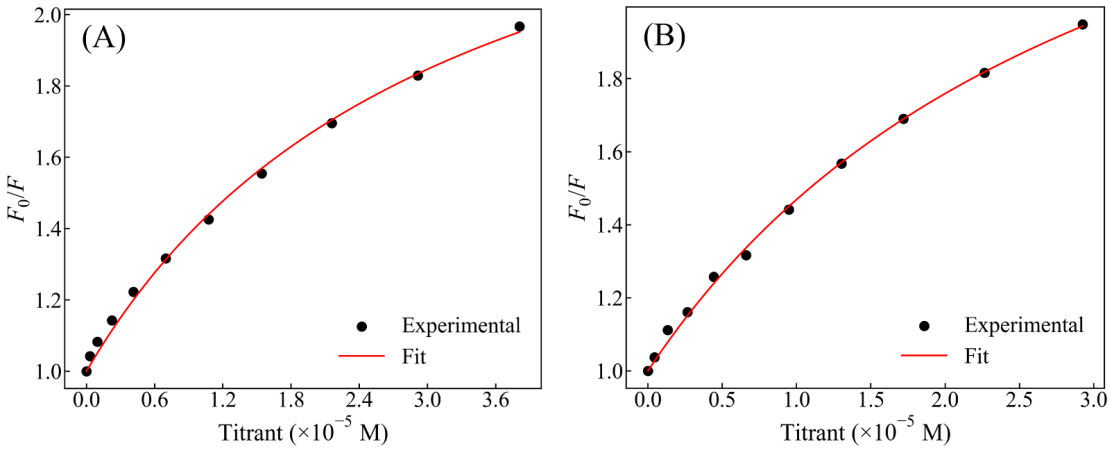

Figure S-18: Non-linear fitted Stern–Volmer fluorescence quenching plots of BSA with increasing concentrations of (A) **3a** ($a = 1.75 \pm 0.109\times$, $b = 3.21 \times 10^{-5} \pm 3.46 \times 10^{-6}$, R^2 = 0.9966) and (B) **3b** ($a = 1.99 \pm 0.116$, $b = 3.24 \times 10^{-5} \pm 2.96 \times 10^{-6}$, R^2 = 0.9980). Measurements for (A) and (B) were taken at $\lambda_{ex} = 277$ nm.

7.2 Molecular Docking Simulations with BSA

Table S-14: Summary of the first two highest-scoring docked structures for compounds **2a/b–3a/b** with the Chain A of BSA (E_b: binding energy, K_d: dissociation constant)

Entry	Dock Site	E_b (kcal/mol)	K_d (nM)	Contacting Receptor Residues
2a	1	10.39	24.13	A GLN 33 A TYR 84 A GLY 85 A ASP 86 A SER 104 A HIS 105 A LYS 106 A ASP 107 A ASP 108 A SER 109 A ARG 196 A LYS 204 A VAL 461 A GLU 464 A LYS 465
	2	10.32	27.43	A GLU 17 A HIS 18 A PHE 126 A GLU 130 A LYS 131 A TRP 134 A ASN 158 A ASN 161 A GLY 162 A GLN 165 A PRO 281
2b	1	9.555	99.10	A LEU 397 A GLY 398 A GLU 399 A TYR 400 A GLY 401 A ILE 512 A ASP 517 A LYS 520 A GLN 521 A LYS 524 A LYS 544 A MET 547 A GLU 548 A PHE 550 A VAL 551 A VAL 554 A ASP 555
	2	8.944	277.9	A GLU 395 A LYS 396 A LEU 397 A GLY 398 A GLU 399 A TYR 400 A GLN 521 A LYS 524 A LYS 544 A MET 547 A GLU 548 A VAL 551
3a	1	9.936	52.10	A LEU 397 A GLY 398 A TYR 400 A GLY 401 A ILE 512 A ASP 517 A LYS 520 A GLN 521 A LYS 524 A MET 547 A PHE 550 A VAL 551 A VAL 554
	2	9.927	52.89	A GLU 17 A HIS 18 A PHE 126 A GLU 130 A LYS 131 A TRP 134 A ASN 158 A LYS 159 A ASN 161 A GLY 162 A GLN 165 A PRO 281 A GLU 284
3b	1	9.025	242.4	A GLU 395 A LYS 396 A LEU 397 A GLY 398 A GLU 399 A TYR 400 A GLN 521 A LYS 524 A LYS 544 A MET 547 A GLU 548 A VAL 551
	2	8.858	321.4	A LEU 397 A GLY 398 A GLU 399 A TYR 400 A GLY 401 A ASN 404 A ILE 512 A ASP 517 A LYS 520 A GLN 521 A LYS 524 A LYS 544 A MET 547 A GLU 548 A PHE 550 A VAL 551 A VAL 554 A ASP 555

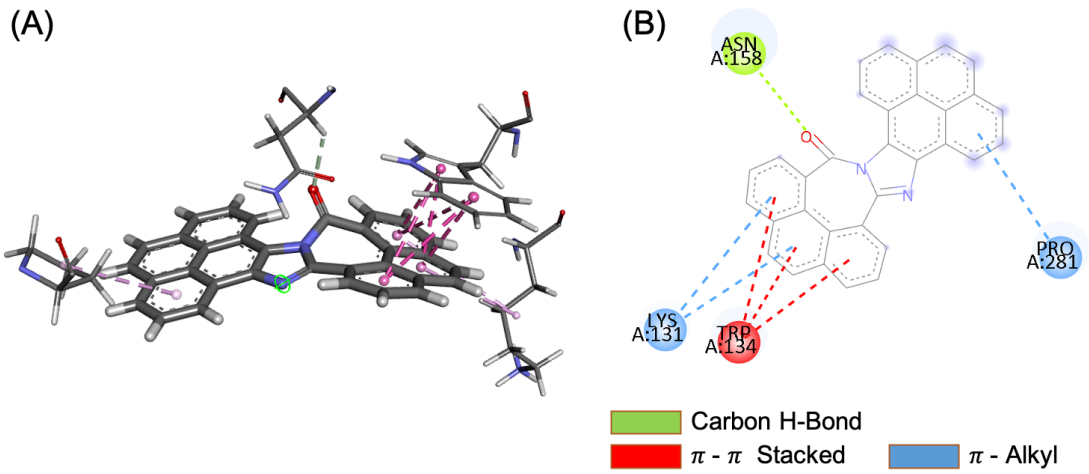

Figure S-19: (A) 3D molecular docking model of compound **2a** showing interactions with key amino acid residues at the BSA docking site corresponding to the second highest binding energy. (B) 2D schematic representation highlighting the major amino acid interactions between **2a** and the same high-affinity BSA binding site.

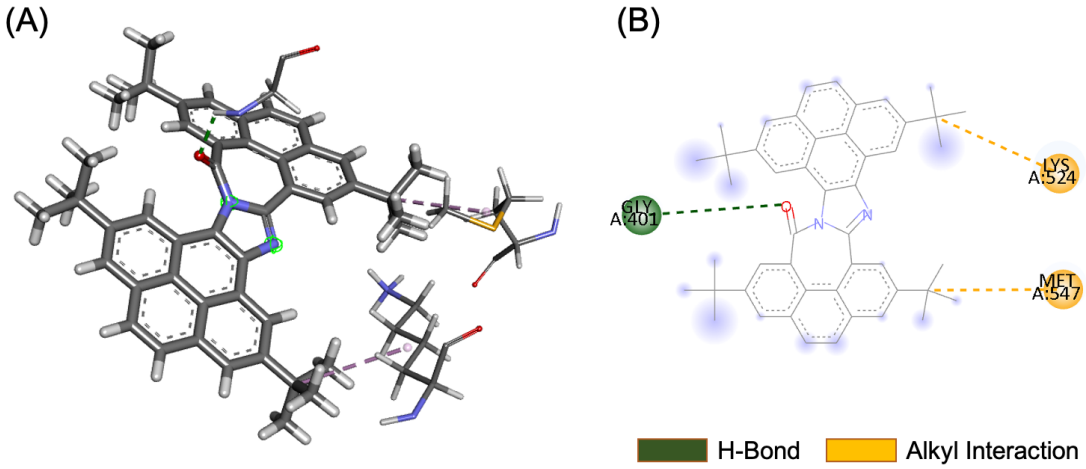

Figure S-20: (A) 3D molecular docking model of compound **2b** showing interactions with key amino acid residues at the BSA docking site corresponding to the second highest binding energy. (B) 2D schematic representation highlighting the major amino acid interactions between **2b** and the same high-affinity BSA binding site.

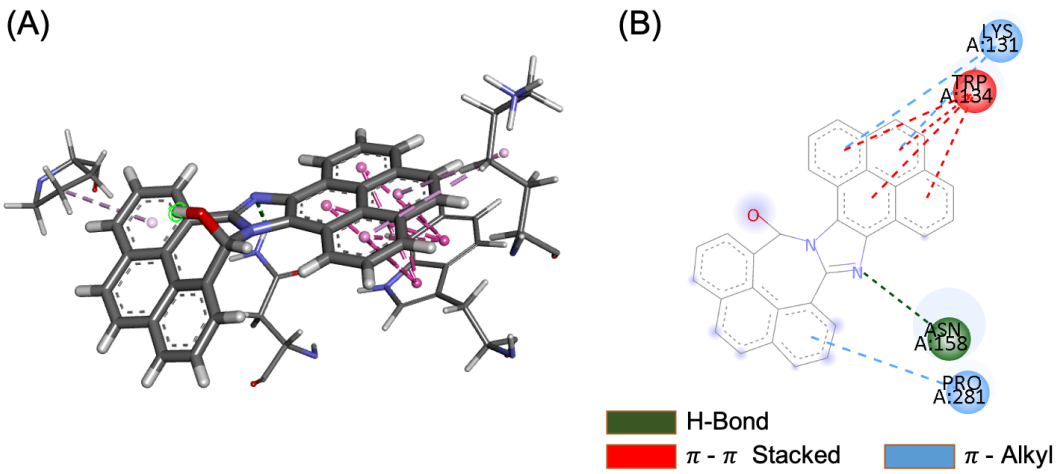

Figure S-21: (A) 3D molecular docking model of compound **3a** showing interactions with key amino acid residues at the BSA docking site corresponding to the second highest binding energy. (B) 2D schematic representation highlighting the major amino acid interactions between **3a** and the same high-affinity BSA binding site.

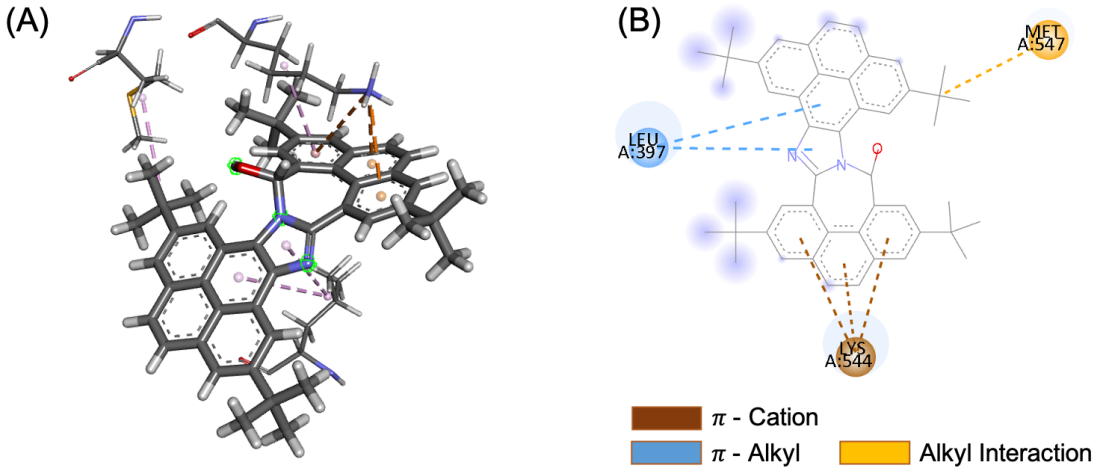

Figure S-22: (A) 3D molecular docking model of compound **3b** showing interactions with key amino acid residues at the BSA docking site corresponding to the second highest binding energy. (B) 2D schematic representation highlighting the major amino acid interactions between **3b** and the same high-affinity BSA binding site.

7.3 Results of MD Simulations

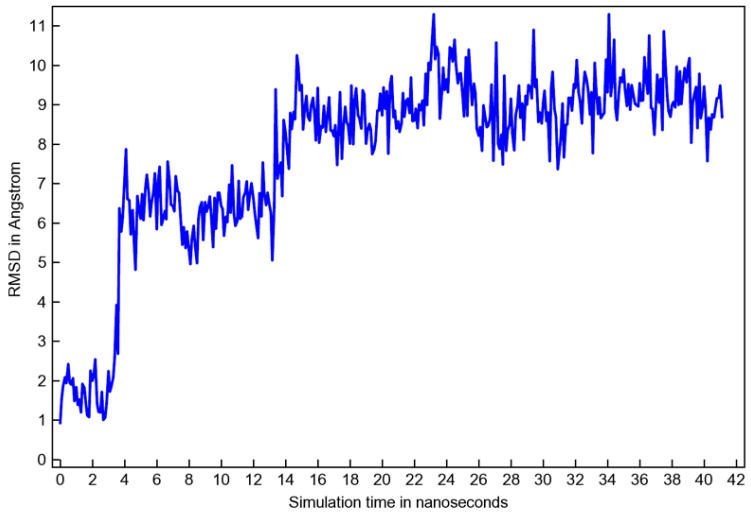

Figure S-23: RMSD plot of **2a** with BSA starting in the second highest binding energy docking site over > 40 ns.

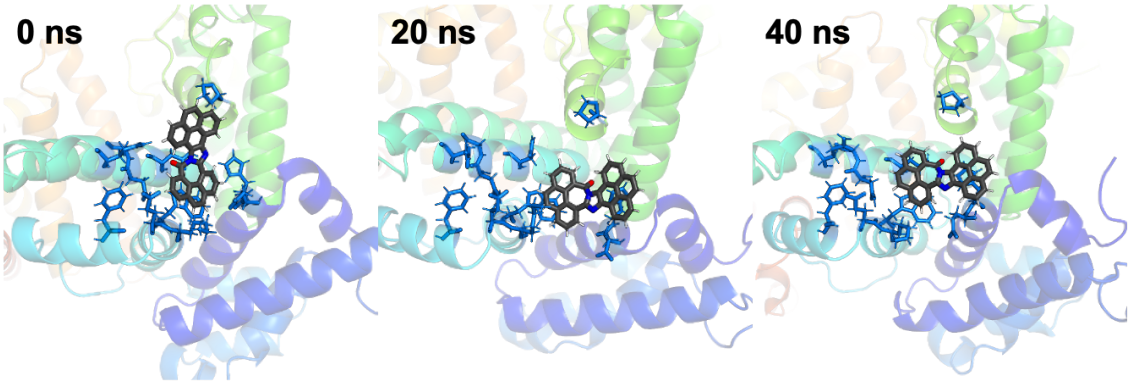

Figure S-24: Binding of **2a** to BSA in the second highest binding energy docking site over time.

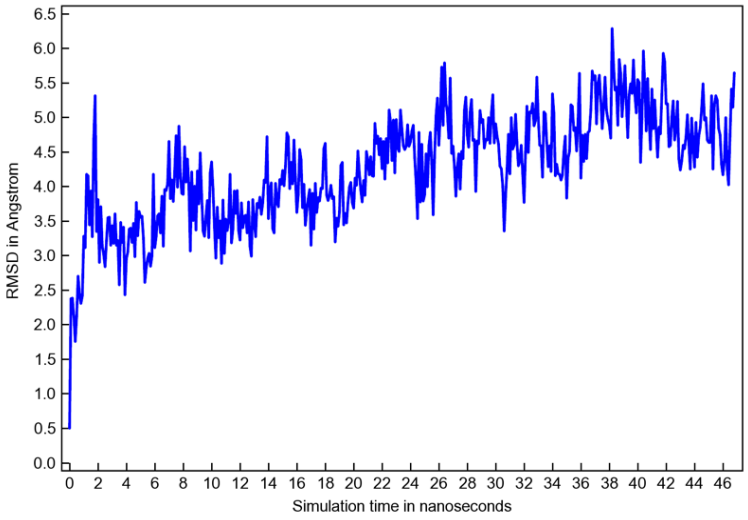

Figure S-25: RMSD plot of **2b** with BSA starting in the second highest binding energy docking site over > 40 ns.

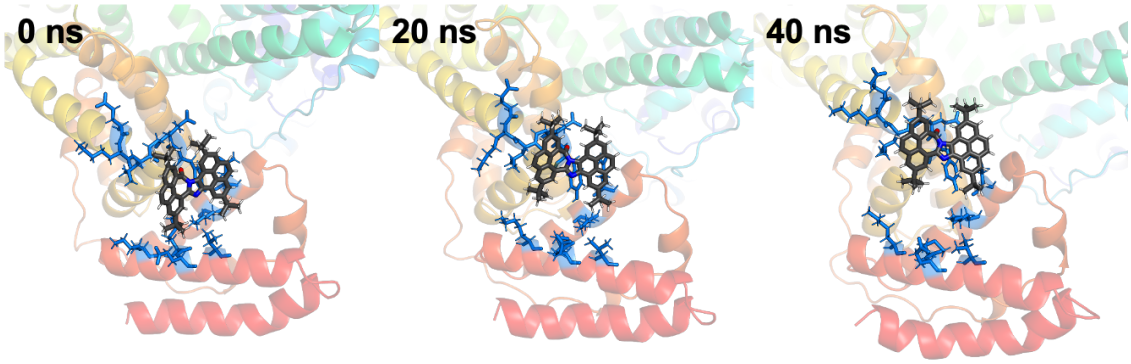

Figure S-26: Binding of **2b** to BSA in the second highest binding energy docking site over time.

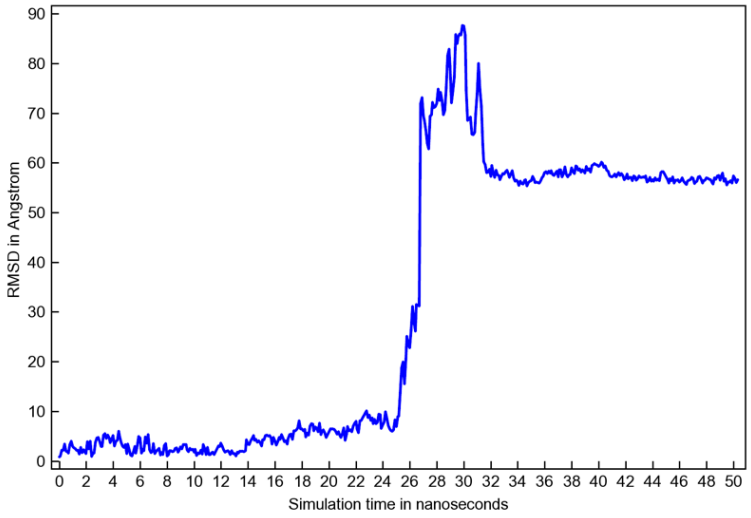

Figure S-27: RMSD plot of **3a** with BSA starting in the second highest binding energy docking site over > 40 ns.

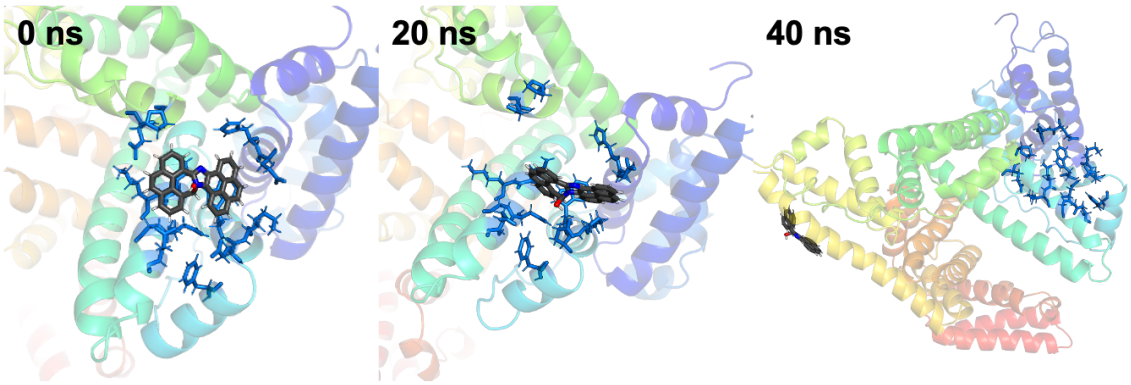

Figure S-28: Binding of **3a** to BSA in the second highest binding energy docking site over time.

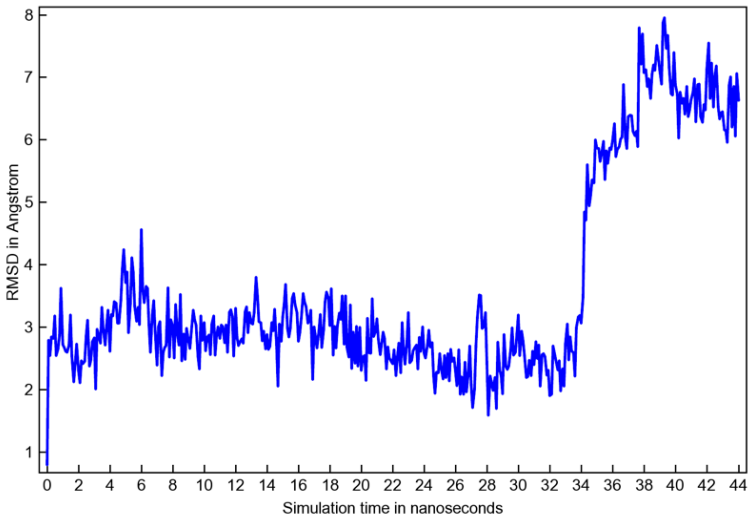

Figure S-29: RMSD plot of **3b** with BSA starting in the second highest binding energy docking site over > 40 ns.

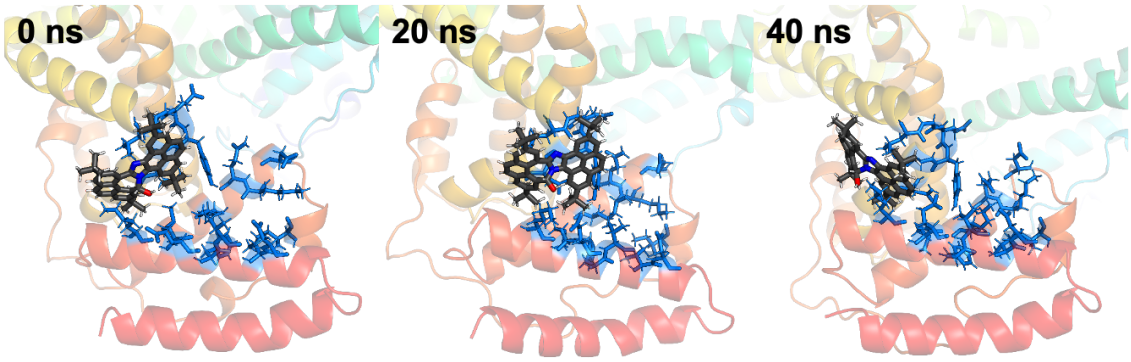

Figure S-30: Binding of **3b** to BSA in the second highest binding energy docking site over time.

References

[1] Walsh, J. C.; Williams, K. M.; Lungerich, D.; Bodwell, G. J. Synthesis of pyrene-4,5-dione on a 15 G scale. *Eur. J. Org. Chem* **2016**, *2016*, 5933—-5936.

[2] Dolomanov, O. V.; Bourhis, L. J.; Gildea, R. J.; Howard, J. A.; Puschmann, H. olex2: A complete structure solution, refinement and Analysis Program. *J. Appl. Crystallogr.* **2009**, *42*, 339—-341.

[3] Sheldrick, G. M. shelxt– integrated space-group and Crystal-structure determination. *Acta Crystallogr., Sect. A: Found. Adv.* **2015**, *71*, 3—-8.

[4] Sheldrick, G. M. Crystal structure refinement with shelxl. *Acta Crystallogr., Sect. C: Struct. Chem.* **2015**, *71*, 3—-8.

[5] Brouwer, A. M. Standards for photoluminescence quantum yield measurements in solution (IUPAC Technical Report). *Pure Appl. Chem.* **2011**, *83*, 2213–2228.

[6] Eaton, D. F. Reference materials for fluorescence measurement. *Pure Appl. Chem.* **1988**, *60*, 1107–1114.

[7] Runge, E.; Gross, E. K. Density-functional theory for time-dependent systems. *Phys. Rev. Lett.* **1984**, *52*, 997.

[8] Frisch, M. J. et al. Gaussian~16 Revision C.01. 2016; Gaussian Inc. Wallingford CT.

[9] Zhao, Y.; Truhlar, D. G. Density functionals with broad applicability in chemistry. *Acc. Chem. Res.* **2008**, *41*, 157–167.

[10] Zhao, Y.; Truhlar, D. G. The M06 suite of density functionals for main group thermochemistry, thermochemical kinetics, noncovalent interactions, excited states, and transition elements: two new functionals and systematic testing of four M06-class functionals and 12 other functionals. *Theor. Chem. Acc.* **2008**, *120*, 215–241.

[11] Weigend, F.; Ahlrichs, R. Balanced basis sets of split valence, triple zeta valence and quadruple zeta valence quality for H to Rn: Design and assessment of accuracy. *Phys. Chem. Chem. Phys.* **2005**, *7*, 3297–3305.

[12] Weigend, F. Accurate Coulomb-fitting basis sets for H to Rn. *Phys. Chem. Chem. Phys.* **2006**, *8*, 1057–1065.

[13] Miertus, S.; Tomasi, J. Approximate evaluations of the electrostatic free energy and internal energy changes in solution processes. *Chem. Phys.* **1982**, *65*, 239–245.

[14] Miertuš, S.; Scrocco, E.; Tomasi, J. Electrostatic interaction of a solute with a continuum. A direct utilizaion of AB initio molecular potentials for the prevision of solvent effects. *Chem. Phys.* **1981**, *55*, 117–129.

[15] Barone, V.; Cossi, M. Quantum calculation of molecular energies and energy gradients in solution by a conductor solvent model. *J. Phys. Chem. A* **1998**, *102*, 1995–2001.

[16] Pascual-ahuir, J.-L.; Silla, E.; Tunon, I. GEPOL: An improved description of molecular surfaces. III. A new algorithm for the computation of a solvent-excluding surface. *J. Comput. Chem.* **1994**, *15*, 1127–1138.

[17] Schrödinger, LLC Available at `https://pymol.org`.

[18] Pettersen, E. F.; Goddard, T. D.; Huang, C. C.; Meng, E. C.; Couch, G. S.; Croll, T. I.; Morris, J. H.; Ferrin, T. E. UCSF ChimeraX: Structure visualization for researchers, educators, and developers. *Protein Sci.* **2021**, *30*, 70–82.

[19] Humphrey, W.; Dalke, A.; Schulten, K. VMD – Visual Molecular Dynamics. *J. Mol. Graph.* **1996**, *14*, 33–38.

[20] Lakowicz, J. R. *Principles of Fluorescence Spectroscopy*, 3rd ed.; Springer, 2006.

[21] Valeur, B.; Berberan-Santos, M. N. *Molecular Fluorescence: Principles and Applications*; Wiley-VCH, 2012.

[22] Royer, C. A. Probing Protein Folding and Conformational Transitions with Fluorescence. *Chem. Rev.* **2006**, *106*, 1769–1784.

[23] Cai, Q.; Ye, X.; Chen, B.; Zhang, B. Complete genome sequence of Exiguobacterium sp. strain N4-1P, a psychrophilic bioemulsifier producer isolated from a cold marine environment in north atlantic Canada. *Genome Announc.* **2017**, *5*, 10–1128.

[24] Land, H.; Svedendahl Humble, M. In *Protein Engineering: Methods and Protocols*; Bornscheuer, U. T., Höhne, M., Eds.; Methods in Molecular Biology; Humana Press: New York, 2018; Vol. 1685; pp 43–67.

[25] BIOVIA, Dassault Systèmes Discovery Studio Visualizer, v20.1.0. 2019; Available at `https://www.3ds.com/products-services/biovia/`.

[26] Shahrokhi, F.; Zhao, Y. Self-condensation of pyrene-4,5-dione: An approach to generate functional organic fluorophores. *Org. Lett.* **2019**, *21*, 9306—-9310.